Biosensors and Bioelectronics 227 (2023) 115177

Contents lists available at ScienceDirect

Biosensors and Bioelectronics

journal homepage: www.elsevier.com/locate/bios

A clinically feasible diagnostic spectro-histology built on SERS-nanotags for multiplex detection and grading of breast cancer biomarkers

Vishnu Priya Murali [a,1], Varsha Karunakaran [a,c,1], Madhukrishnan Murali [a,c], Asha Lekshmi [d], Shamna Kottarathil [a], Selvakumar Deepika [a], Valliamma N. Saritha [d], Adukkadan N. Ramya [a,c], Kozhiparambil G. Raghu [b,c], Kunjuraman Sujathan [d,**], Kaustabh Kumar Maiti [a,c,*]

[a] CSIR-National Institute for Interdisciplinary Science & Technology (NIIST), Chemical Sciences & Technology Division (CSTD), Organic Chemistry Section, Industrial Estate, Thiruvananthapuram, 695019, Kerala, India
[b] CSIR-National Institute for Interdisciplinary Science & Technology (NIIST), Agro-Processing and Technology Division (APTD), Industrial Estate, Thiruvananthapuram, 695019, Kerala, India
[c] Academy of Scientific and Innovative Research (AcSIR), Ghaziabad, 201002, India
[d] Regional Cancer Centre (RCC), Division of Cancer Research, Thiruvananthapuram, 695011, Kerala, India

ARTICLE INFO

Keywords:
Breast cancer
Biomarkers
SERS nanotags
Multiplex detection
HER2 grading
Immunohistochemistry

ABSTRACT

Simultaneous detection of multiple biomarkers is always an obstacle in immunohistochemical (IHC) analysis. Herein, a straightforward spectroscopy-driven histopathologic approach has emerged as a paradigm of Raman-label (RL) nanoparticle probes for multiplex recognition of pertinent biomarkers in heterogeneous breast cancer. The nanoprobes are constructed by sequential incorporation of signature RL and target specific antibodies on gold nanoparticles, which are coined as Raman-Label surface enhanced Raman scattering (RL-SERS)-nanotags to evaluate simultaneous recognition of clinically relevant breast cancer biomarkers i.e., estrogen receptor (ER), progesterone receptor (PR) and human epidermal growth factor receptor2 (HER2). As a foot-step assessment, breast cancer cell lines having varied expression levels of the triple biomarkers are investigated. Subsequently, the optimized detection strategy using RL-SERS-nanotags is subjected to clinically confirmed, retrospective formalin-fixed paraffin embedded (FFPE) breast cancer tissue samples to fish out the quick response of singleplex, duplex as well as triplex biomarkers in a single tissue specimen by adopting a ratiometric signature RL-SERS analysis which enabled to minimize the false negative and positive results. Significantly, sensitivity and specificity of 95% and 92% for singleplex, 88% and 85% for duplex, and 75% and 67% for triplex biomarker has been achieved by assessing specific Raman fingerprints of the respective SERS-tags. Furthermore, a semi-quantitative evaluation of HER2 grading between 4+/2+/1+ tissue samples was also achieved by the Raman intensity profiling of the SERS-tag, which is fully in agreement with the expensive fluorescent in situ hybridization analysis. Additionally, the practical diagnostic applicability of RL-SERS-tags has been achieved by large area SERS imaging of areas covering 0.5–5 mm2 within 45 min. These findings unveil an accurate, inexpensive and multiplex diagnostic modality envisaging large-scale multi-centric clinical validation.

1. Introduction

Clinical biomarkers partake an imperative role in breast cancer prognosis and its heterogenous as well as differential expression pattern exhibit the key challenge in choosing the proper treatment modality. Hence, breast cancer biomarker detection prevails the decisive feature which needs a distinct troubleshooting approach (Shah et al., 2014). The three vital prognostic markers widely assessed in breast cancer diagnosis includes hormonal nuclear receptors estrogen (ER) (Russo and Russo, 2006), progesterone (Lange, 2008) and cell surface human epidermal growth factor type 2/neu (HER2/neu) receptors (Costa and Czerniecki, 2020). Based on these biomarker expression profiles, four major

* Corresponding author. CSIR-National Institute for Interdisciplinary Science & Technology (NIIST), Chemical Sciences & Technology Division (CSTD), Organic Chemistry Section, Industrial Estate, Thiruvananthapuram, 695019, Kerala, India.
** Corresponding author.
E-mail addresses: ksujathan@gmail.com (K. Sujathan), kkmaiti@niist.res.in (K.K. Maiti).
[1] Both the authors contributed equally to this work.

https://doi.org/10.1016/j.bios.2023.115177
Received 9 November 2022; Received in revised form 14 February 2023; Accepted 22 February 2023
Available online 25 February 2023

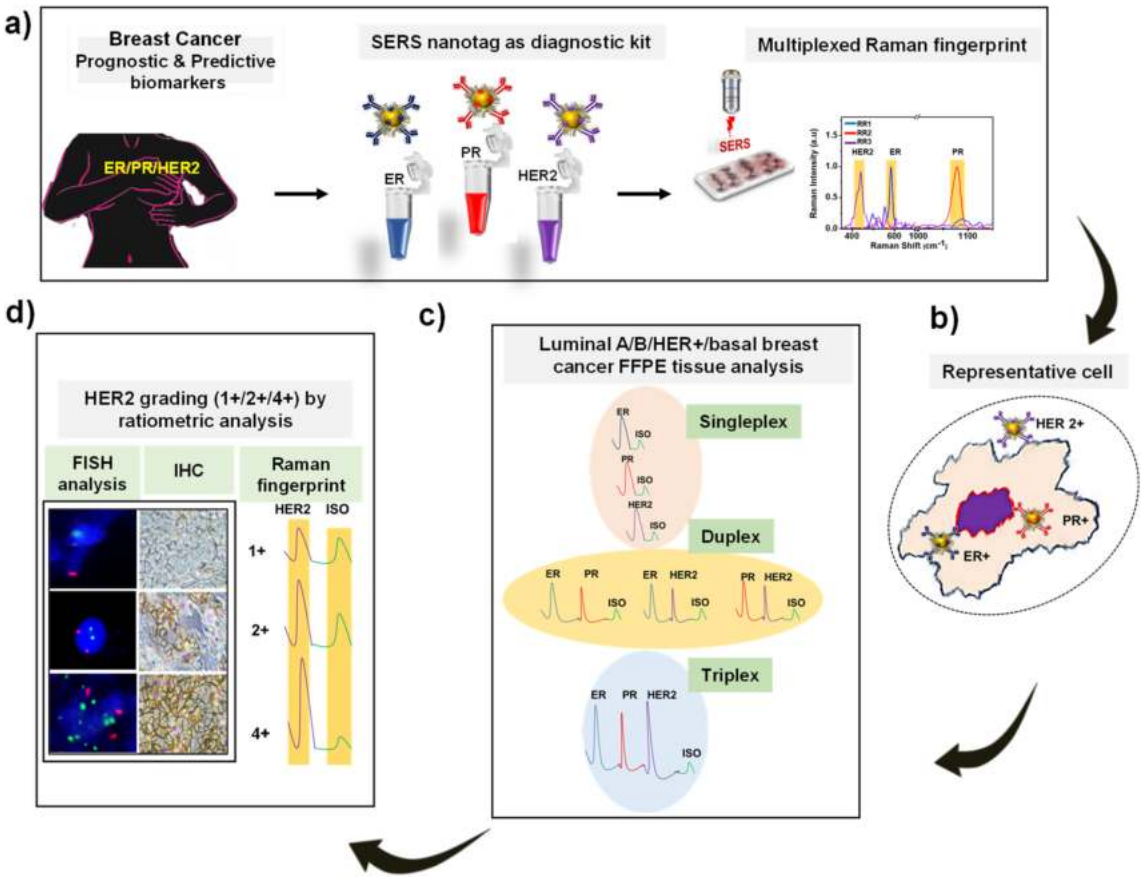

Scheme 1. Schematic illustration of the experimental design for differentiating the clinically relevant triple biomarkers, ER, PR and HER2. a) strategy for the multiplexed detection using ER, PR and HER2 conjugated SERS-tags having AuNPs as substrate, b) representative design for detection of biomarkers in cells/paraffin embedded breast tissue samples using SERS mapping, c) Three phases of biomarker detection executed as single, dual and triple biomarker analysis from the breast tissue specimens, d) HER2 grading of IHC and FISH confirmed 1^+, 2^+ and 4^+ tissue sample through ratiometric SERS mapping.

classification of breast cancer are designated, viz., luminal A, luminal B, HER2 enriched and basal like subtypes (Parise and Caggiano, 2014). The occurrence and extend of cell surface biomarker HER2 is often measured by a grading system having 4^+, 3^+, 2^+, 1^+ and 0 grades correlating the staining intensity. According to HER2 testing guidelines and samples with a staining score of 2^+ or less is considered as negative (Cornejo et al., 2014). The gold standard method immunohistochemistry (IHC), which is generally employed for the detection of these biomarkers is relatively inexpensive, but the results are often subjective as influenced by inter-observer variability. Besides, evaluation of multiple biomarkers simultaneously in a single tissue specimen is not possible, which turned out as a lengthy process to complete the investigation of all three-biomarker status (Dixon et al., 2015). In the case of HER2 detection, 95% concordance is mandatory within IHC and Fluorescent in situ hybridization (FISH). FISH is a cytogenic analysis to detect the number of HER2 gene copies per nucleus. Even though FISH is a robust technique for HER2 detection, it necessitates expensive reagents along with laboratory equipment setup (Bogdanovska-Todorovska et al., 2018; Furrer et al., 2015; Wesoła and Jeleń, 2015). Besides, techniques like multiplex immunohistochemistry/immunofluorescence (mIHC/mIF) have been introduced as improved methods to detect multiple biomarkers in single tissue section, its applicability has been restricted due to several disadvantages like, limited dynamic range for intensity of the chromogenic substrates in mIHC. On the other hand, mIF has a large linear dynamic range for many fluorophores for quantitative analysis, however, they must be chosen carefully for preventing bleed through. The highly sensitive tyramide signal amplification (TSA) method is also insubstantial due to the complicated steps involved, tyranide overaction and its time consuming nature (Hernandez et al., 2021; Sheng et al., 2023; Tan et al., 2020). Exploration and validation of alternative simple and relatively rapid techniques are always recommended which can meet acceptable diagnostic quality.

Surface enhanced Raman spectroscopy (SERS), is an advanced and ultrasensitive technique which received immense scientific attention especially in diverse clinical diagnostic applications including cancer in last several years (Haka et al., 2005; Ramya et al., 2021) (Joseph et al., 2018). The efficient optical properties of Raman labels possessing narrow bandwidth of the Raman peaks boosts its potential for spectral multiplexing unlike quantum dots (Qds) and fluorescent dyes. SERS-nanotags or SERS-nanoprobes are prepared by incorporating Raman reporter molecules enabling inherently strong Raman cross-section to plasmon resonant metallic nanoparticles like gold or silver. Subsequently, a protective polymeric layer and a target specific recognition motif like a peptide, antibody or aptamer are functionalized to the SERS-nanotags which exclusively recognize specific biomarkers *in vitro*, *in vivo* and *ex vivo* specimens having moderately high heterogeneity (Wang et al., 2013).

Sensitive singleplex/multiplex detection of clinically relevant cancer biomarkers utilizing SERS-nanotags has shown a very promising alternative strategy, stepping up towards the upcoming technology for clinical diagnostics (Dinish et al., 2014; Nariman et al., 2017; Sun et al., 2021). Hence, SERS-nanotags resemble an ideal SERS-based immunoassay component for the precise detection of multiplex biomarkers in a personalized manner with high sensitivity and specificity (Schlücker et al., 2011).

Even though a few SERS-based multiplexed studies have been

demonstrated for other cancer types (Davis et al., 2018; Lin et al., 2021; Maiti et al., 2012; Narayanan et al., 2015; Zavaleta et al., 2013) as well as breast cancer biomarkers in cells (Lee et al., 2014), serum (Li et al., 2015) and fresh tissue (Wang et al., 2017) etc., there is no report so far on multiplex detection of three prevalent prognostic markersi.e., ER, PR and HER2 in a single tissue sample as a complementary system to IHC as well as FISH analysis. Similarly, biomarker detection in fresh tissue samples via topical application of SERS-tags followed by raster scanning to determine surgical margin during lumpectomy has also been investigated (Y. Y. Wang et al., 2016; Y. W. Y.W. Wang et al., 2016), whereas the present study prevails its distinct feature of biomarker detection in the retrospective formalin fixed paraffin embedded breast tissue specimens as a parallel platform that envisages to nullify the highly time consuming and subjective nature of immunohistochemistry and expensive FISH technique.

Herein, we have evaluated the clinical implementation of the multiplexing capability of the SERS technique using multiplex Raman-label SERS (RL-SERS)-nanotags to determine the breast cancer prognostic biomarkers, ER/PR/HER2 complementary to IHC. The preeminence of the study over the so far reported SERS multiplexing studies includes the clinical relevance of the selected biomarkers and its detection in FFPE specimens, time efficient approach to analyze the maximum area of tissue samples by ratiometric large area scanning and the analysis of an ambient number of different tissue subtypes in terms of biomarker status. Moreover, this is the first-ever report on the semi-quantitative evaluation of HER2 grading between 4+/2+/1+ tissue samples by ratiometric SERS intensity profiling, in concordance with FISH analysis (Scheme 1). Collectively, to establish the utility of SERS-nanotags as a next-generation clinical diagnostic modality enabling a fast, facile, accurate, and reliable spectro-histologic technique for multiplex prognostic analysis of heterogenous breast cancer biomarkers.

2. Results and discussion

2.1. SERS-nanotags (SERS-nanotags) for multiplex detection

Gold nanoparticles (AuNPs: 40–45 nm) were selected as a SERS substrate for the preparation of SERS-nanotags to perform the multiplexing recognition of ER, PR and HER2 in breast cancer due to its excellent SERS enhancement reported so far (Njoki et al., 2007). The synthesized SERS substrate was characterized by UV–vis Spectroscopy, Dynamic Light Scattering (DLS) and High-Resolution Transmission Electron Microscopy (HR-TEM) analysis (Figure S1a, b and c). Further, SERS-nanotags were fabricated by tagging Raman labels (reporters) having multiplexed Raman peaks which were designated *w.r.t.,* each breast cancer biomarker by the respective Raman signature peak of the reporter molecule. Among three Raman reporters, commercially purchased crystal violet (CV) and 4-mercapto benzoic acid (MBA) were chosen based on multiplex Raman peaks at 440 and 1084 cm^{-1} respectively, along with the in-house synthesized Raman reporter, squaraine di-lipoic acid (SDL) (Ramya et al., 2015) with a non-overlap Raman peak at 580 cm^{-1} *w.r.t* CV and MBA.

The structure and the SERS fingerprint pattern of the three SERS nanotags were portrayed in Figs. S2a, b, c and d. Isotype antibody conjugated SERS-tags were prepared independently with Dithio nitrobenzoic acid (DTNB) as well as 3,3 -Diethylthiacarbocyanine iodide (DTTC) having signature Raman peak at 1320 cm^{-1} and 505 cm^{-1} respectively (Figs. S2e and f). The stability and biocompatibility of nanotags were improved by a protective layer of polyethylene glycol (PEG) and the carboxy functionalized PEG which facilitated the conjugation of target-specific antibodies. UV–Vis spectroscopy, TEM and DLS analysis of the PEGylated nanoparticles were also accomplished to confirm the PEG layer formation (Figure S1d, e and f). The stickiness nature and aggregation tendency of nanoparticles were minimized with the employment of Tween 20 (Lin et al., 2010). The biocompatibility of the fabricated RL-SERS-tags was further confirmed by cell viability assay in different breast cancer cell lines (Fig. S3 a, b and c). The simultaneous detection of breast cancer biomarkers was executed by constructing three multiplexing RL-SERS-nanotags conjugated with the specific monoclonal antibodies for the detection of clinically valid biomarkers i.e., ER, PR and HER2. The successful conjugation of antibodies to AuNPs was confirmed by UV–Vis absorbance (Fig. S4 a,b,c) which showed a protein absorption peak around 280 nm without much compromise in the SERS activity (Fig. S4 d,e,f). Besides, polyacrylamide gel electrophoresis (PAGE) analysis (Figs. S5a,b,c) and 3, 3′, 5, 5′ Tetramethylbenzidine (TMB) assay (Figure S5 d) also confirmed the presence of the tethered antibodies on the SERS-nanotags. The stability of the SERS-nanotags was also monitored up to six months which ensured the stability of the nanotags based on consistant SERS intensity of the signature peaks. (Fig. S6).

2.2. Multiplex detection by SERS-nanotags in ER, PR and HER2 overexpressed breast cancer cells (phase I)

As a proof-of-principle of multiplex detection, the RL-SERS-nanotags have endeavoured in breast cancer cell lines. To accomplish this, immunophenotyping was performed to ensure the ER and PR abundance in MCF-7 cells as well as HER2 over-expression in SK-BR-3 cells and compared with the triple negative MDA-MB-231 cells (Figure S7a, b and c). Further, incubation time of SERS-nanotag was optimized within 2 h (Fig. S8). SERS analysis of MCF-7 (luminal A subtype, ER^{+}/PR^{+}), after incubating with AuNP@SDL@anti-ER, AuNP@MBA@anti-PR and AuNP@CV@anti HER2 SERS-nanotags identified the protuberant Raman signature peaks of the Raman labels SDL at 580 and MBA at 1084 cm^{-1} from the nuclear location without any prominent CV peak at 440 cm^{-1} from the whole cell demonstrating the effective recognition of ER and PR (Fig. S9 a-d). Similarly, upon incubation of all three nanotags with HER2-enriched breast cancer subtype SK-BR-3, resulted the presence of noticeable Raman peak of CV (crystal violet) at 440 cm^{-1} from the cell surface milieu (Fig. S10 a-d). Similarly, a basal subtype (ER^{+}/PR^{+}/$HER2^{+}$triple negative receptors) MDA-MB-231 cell line resembled a negligible expression as indicated from all the three RL-SERS-nanotags ensuring the specificity of the nanotags (Figure S11a,b and c). A parallel confirmation has been carried out for the recognition of biomarkers through RL-SERS-nanotags, by dark field microscopic analysis based on the back scattering property of the metallic nanoparticle uptake as detailed in the supporting information (Fig. S12 a, b and c).

2.3. Multiplex detection strategy in clinically confirmed breast tissue samples

After the proof-of-concept confirmation in breast cancer cell lines, analysis in retrospective clinical FFPE tissue sections accumulated from lumpectomy/mastectomy-derived specimens was performed for the SERS detection of ER, PR, and HER2 biomarkers. Ratiometric SERS evaluation was executed to detect the presence of single and multiple biomarkers, with non-targeted IgG isotype antibody conjugated SERS-tags along with the targeted ones as a control to minimize the false positive signal arising due to the non-specific binding. For attaining these goals, three sets of detection modes were executed viz., singleplex i.e., detection of single biomarkers either ER, PR or HER2 individually, then duplex with a combination of any two out of three biomarkers and triplex analysis, which aimed to detect the expression status of all the three biomarkers simultaneously in a single tissue specimen.

2.3.1. Singleplex analysis of tissue biomarkers by SERS-nanotags

The first stage of clinical sample analysis was envisioned to detect a single biomarker either ER/PR/HER2 in FFPE breast cancer tissue specimens. One of the major challenging factors in the detection technique was the nonspecific binding of nanotags to the specimen, which may lead to false positive results (Fig. S13), thus reducing the specificity of the detection model. To circumvent this stipulation, we have

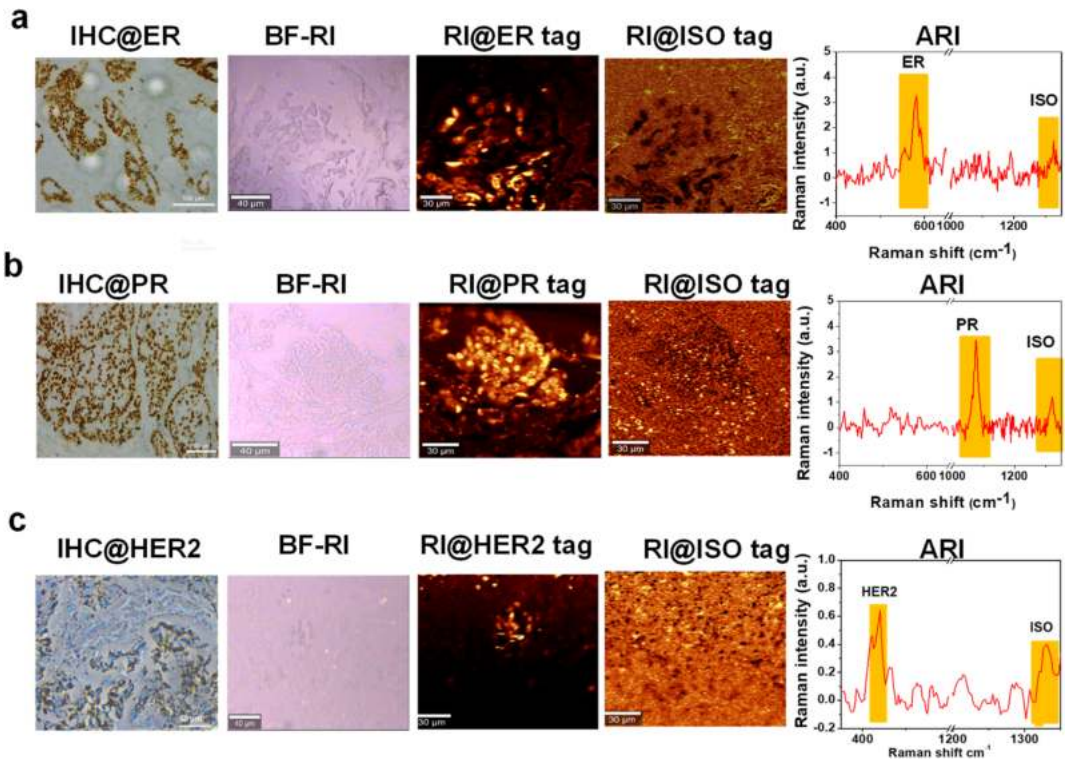

Fig. 1. SERS singleplex analysis of a) ER^+ b) PR^+ and c) $HER2^+$ tissue using AuNP@SDL@PEG@anti-ER, AuNP@MBA@PEG@anti-PR and AuNP@CV@PEG@anti-HER2 nanotags along with AuNP@DTNB@PEG@anti-isotype tag. IHC-Immunohistochemistry confirmation for ER, PR and HER2 positivity of the specimens, BF-RI-Bright field images of the tissue area subjected for Raman image scanning, RI-Raman image corresponds to (a) 580 cm^{-1} of AuNP@SDL@PEG@anti-ER, (b) corresponds to 1084 cm^{-1} of AuNP@MBA@PEG@anti-PR and (c) corresponds to AuNP@CV@PEG@anti-HER2, RI@ISO tag corresponds the Raman images of AuNP@DTNB@PEG@anti-isotype., ARI-Average Raman intensity from the average scan spectrum of the ER^+, PR^+ and $HER2^+$ tissue samples respectively.

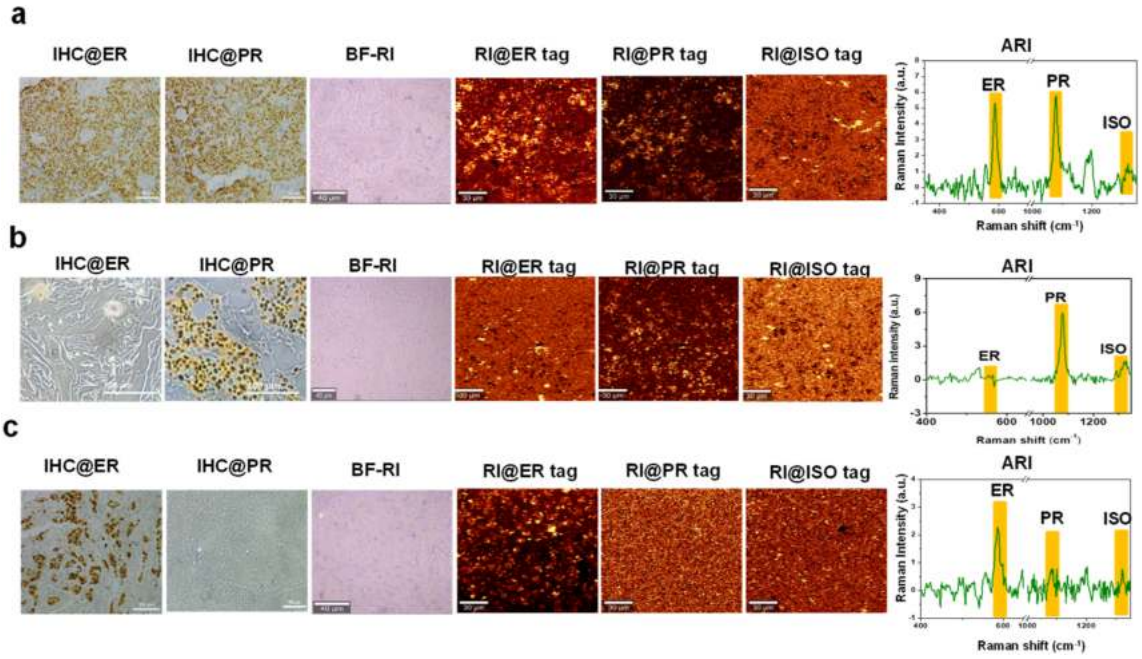

Fig. 2. SERS duplex analysis of a) of ER^+ and PR^+ tissue, b) ER^- and PR^+ tissue and c) ER^+ and PR^- tissue samples using AuNP@SDL@PEG@anti-ER, AuNP@MBA@PEG@anti-PR and AuNP@CV@PEG@anti-HER2 nanotags along with AuNP@DTNB@PEG@anti-isotype tag. IHC-Immunohistochemistry confirmation for ER, PR and HER2 positivity of the specimens, BF-RI- Bright field images of the tissue area subjected for Raman image scanning, RI-Raman image corresponds to (a) 580 cm^{-1} of AuNP@SDL@PEG@anti-ER, (b) corresponds to 1084 cm^{-1} of AuNP@MBA@PEG@anti-PR and (c) corresponds to AuNP@CV@PEG@anti-HER2, RI@ISO tag corresponds the Raman images of AuNP@DTNB@PEG@anti-isotype, ARI-Average Raman intensity from the scan spectrum.

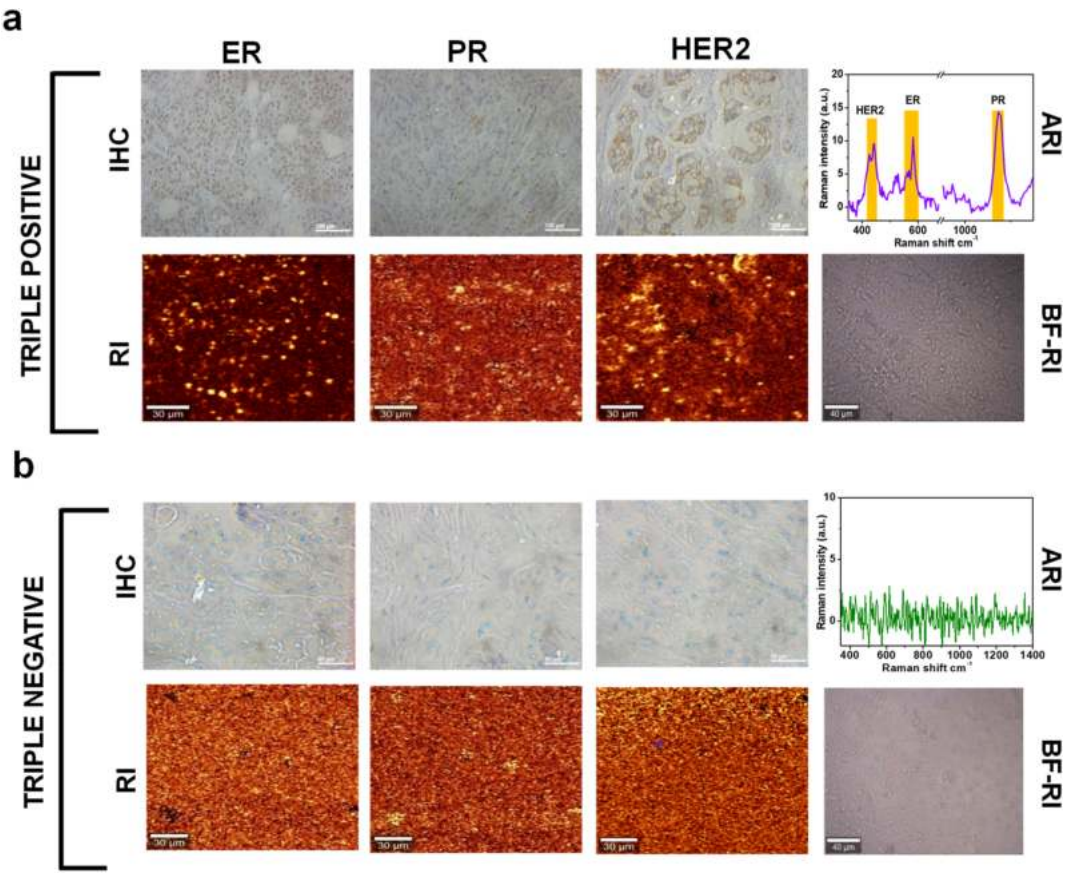

Fig. 3. SERS analysis of a) Luminal B ($ER^+PR^+HER2^+$) and b) Basal (ER-PR-HER2-) tissue using AuNP@SDL@anti-ER, AuNP@MBA@anti-PR and AuNP@CV@anti-HER2 nanotags. IHC-Immunohistochemistry confirmation for ER, PR and HER2 positivity of the specimens, BF-RI- Bright field images of the tissue area subjected for Raman image scanning, RI-Raman image corresponds to (a) 580 cm^{-1} of AuNP@SDL@PEG@anti-ER, 1084 cm^{-1} of AuNP@MBA@PEG@anti-PR and 440 cm^{-1} of AuNP@CV@PEG@anti-HER2, ARI-Average Raman intensity denotes the average scan spectrum of the duplex biomarkers in tissue samples respectively.

introduced an isotype antibody (IgG) conjugated SERS-tag as a control with the respective singleplex nanotag (Wang et al., 2014) that provided a ratiometric approach where the ratio of SERS intensity profile of ER/PR/HER2 conjugated SERS-nanotags and isotype control SERS-nanotags were measured. As shown in Fig. 1a, IHC confirmed ER positive tissue treated with AuNP@SDL@anti-ER SERS tag provided a high-resolution Raman image and an average Raman intensity (ARI) corresponding to the signature peak of SDL at 580 cm^{-1} demonstrating the sensitivity of ER nanotag. Similarly, from different experiments, PR (Fig. 1b) and HER2 (Fig. 1c) positive tissues incubated with SERS-nanotag (AuNP@MBA@anti-PR & AuNP@CV@anti-HER2) afforded distinct Raman images and average spectrum with marker reporter peaks at 1084 (MBA) and 440 (CV) cm^{-1} respectively. A ratio less than or equal to one is considered negative for that particular biomarker where as a value greater than one is considered positive (Table S1). Therefore, the formulated methodology by using RL-SERS-nanotags demonstrated a sensitive and specific detection of the corresponding single biomarker in the FFPE breast cancer tissue specimens.

2.3.2. *Duplex analysis for tissue biomarkers by SERS-nanotags*

Even though a few kits-based methods persisted, dual biomarker detection is a still challenging aspect to achieve through IHC. Using the current RL-SERS-tags, we have examined combinations of two biomarker analysis at a time, along with isotype control and investigated the differential expression status in a single tissue specimen. As shown in Fig. 2a, luminal A tissue sample having ER^+ PR^+ expression was treated with SERS-tags conjugated to anti-ER (AuNP@SDL@anti-ER) and anti-PR (AuNP@MBA@anti-PR) antibodies. The average scan spectrum generated from the Raman image symbolized the presence of the signature peaks from SDL at 580 cm^{-1} and MBA at 1084 cm^{-1} with a ratiometric value > 1 as compared to AuNP@DTNB@Isotype confirming the specific recognition of ER and PR. Corresponding receptor negative samples viz., ER^-PR^+ (Fig. 2b) and ER^+PR^- tissues (Fig. 2c) exhibited minimal SERS signals of SDL (580 cm^{-1}) and MBA (1084 cm^{-1}) respectively with a ratiometric value of <1. (Table S2). ER/HER2 and PR/HER2 duplexing were also experimented with to confirm the dual biomarker detection ability of the RL-SERS tags (Figure S 14, Table S3).

2.3.3. *Triplex analysis for tissue biomarkers in luminal B and basal tissue samples by RL-SERS-nanotags*

In the set-up for triplex analysis, IHC confirmed luminal B ($ER^+PR^+HER2^+$) tissue sample was incubated with all the three SERS-nanotags i.e., AuNP@SDL@anti-ER, AuNP@MBA@anti-PR and AuNP@CV@anti-HER2. SERS analysis revealed the recognition of ER, PR and HER2 biomarkers even in a single scan with its average spectrum having corresponding peaks of SERS-nanotags at 580, 1084 and 440 cm^{-1} with scanned images showing the receptor positive and negative areas of the sample corroborating the detection of three biomarkers in a single specimen (Fig. 3a). Further, in another set, where IHC confirmed ER, PR and HER2 negative tissue (basal type) specimen was analysed with the SERS-tags, it showed negligible Raman peaks for the three biomarkers (Fig. 3b). A summarized data of tissue analysis is shown in Table S4.

2.4. *HER-2 grading based on signature Raman label*

Unlike ER and PR, HER2 overexpression is considered for effective targeted therapy by the treatment of clinically approved trastuzumab.

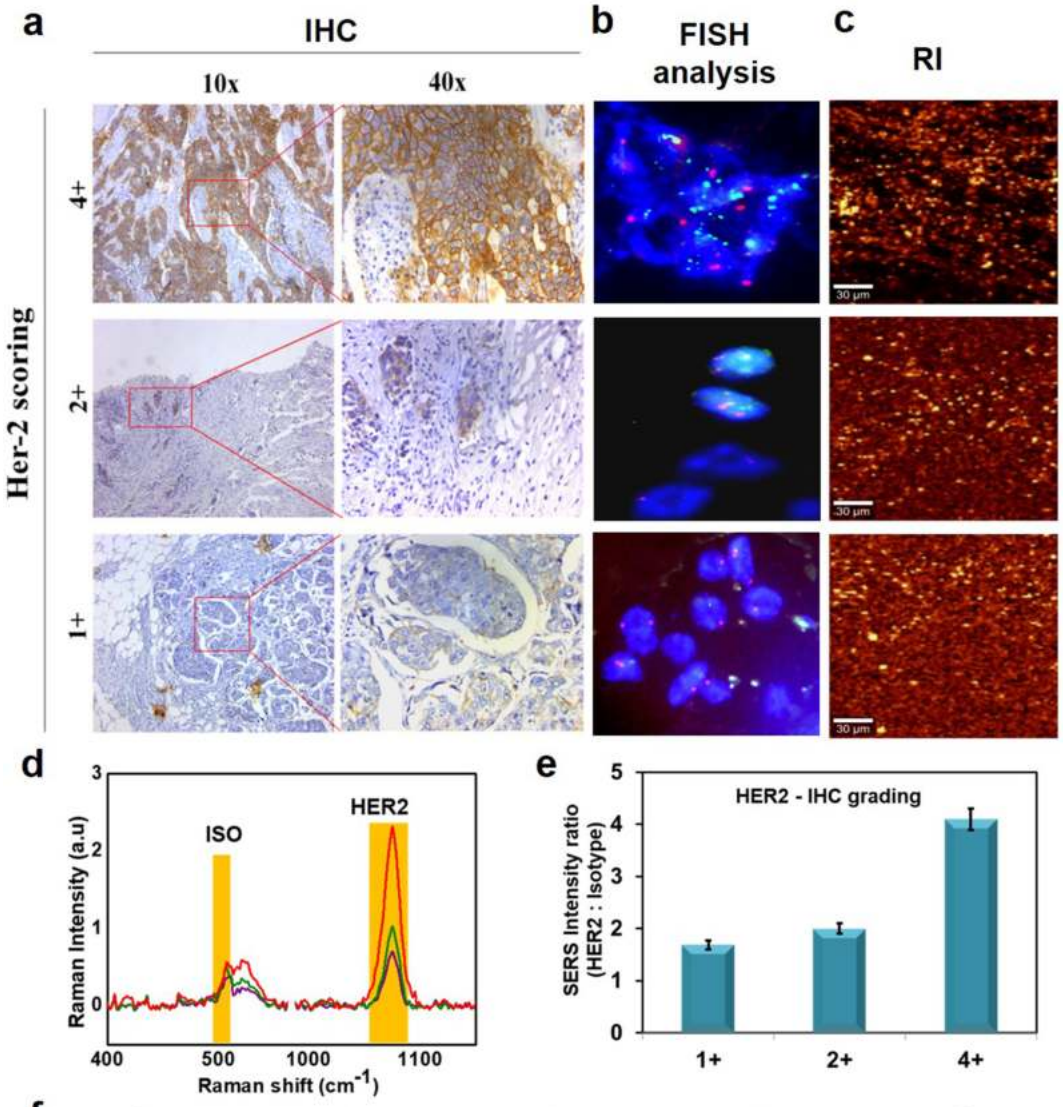

f

HER2 grade	A.R.I HER2	A.R.I Iso	HER2:ISO
1^+	1.19 ± 0.32	0.69 ± 0.20	1.75 ± 0.15
2^+	0.88 ± 0.64	0.40 ± 0.41	2.17 ± 0.20
4^+	3.93 ± 0.82	1.07 ± 0.15	3.67 ± 0.51

Fig. 4. SERS analysis showing HER2 grading in HER2$^+$ tissue using HER2 targeted AuNP@MBA@anti-HER2 and Isotype targeted AuNP@DTTC@anti-isotype nanotags. a) IHC analysis, b) FISH analysis (Orange flourochrome-for centromere (*CEP17)* of chromosome 17 as internal control, Green flourochrome - HER 2 gene),c) Raman Imaging (RI), d) Average Raman Intensity (ARI) and color representations, Purple (HER2 $^{1+}$), Green (HER2 $^{2+}$), Red (HER2 $^{4+}$), e) representation of HER2 grading by bar diagram and f) table showing ratiometric signal values of HER2 versus isotype tags. Data, Average ± SD of three different analysis.

IHC grading of 3^+ and more are judged to be HER2 positive, whereas 2^+/ equivocal expression require further confirmation by FISH (Fluorescent in situ hybridization) analysis in which the number of HER2 gene copies per nucleus is assessed. This method is again a time-consuming and highly expensive technique in cytopathology. We introduced a ratiometric analysis of SERS-nanotag for measuring HER2 grading based on the signature Raman peak which preciously profiled the intensity ratio between HER2-tag and isotype-control-tag. The Raman reporter DTTC was used for the isotype antibody conjugated SERS-nanotag. As indicated in Fig. 4, IHC grades of 1^+, 2^+ and 4^+ tissue samples (Fig. 4a) parallelly confirmed by FISH analysis (Fig. 4b) were treated to Raman-labeled SERS-tag (AuNP@MBA@anti-HER2) and isotype control SERS-tag (AuNP@DTTC@Isotype) to assess the ratiometric analysis. Fig. 4c revealed the Raman scanned image, which indicated the gradation of HER2 expression. The Raman intensity profile of the signature Raman label MBA (1084 cm^{-1}) and DTTC (505 cm^{-1}) designating HER2 -tag and isotype-tag respectively is depicted in Fig. 4d. The ratio of HER2-tag to isotype-tag obtained from the average scan intensities is plotted in a bar diagram to get a mathematical interpretation of the same (Fig. 4e). Average SERS intensity from image scanning was found to be higher for 4^+ HER2 tissue with an intensity ratio of 3.67 ± 0.51 followed by 2^+ HER2 (Ratio: 2.17 ± 0.2) and 1^+ (Ratio: 1.75 ± 0.15) in harmony with

Table 1
Comparative pros and cons analysis of SERS vs IHC.

Criteria	*Pros of SERS over IHC*	
	IHC	SERS
Multiplex detection of biomarkers	Difficult to attain due to the deficiency of standard methods	Easily possible
Sample preparation time	7–24 h	5–6 h
Secondary antibody and developing agents	Required	Not required
Analysis time	0.5 h/sample/one biomarker	1 h/sample with multiple biomarker
Performance/ Precision	Subjective due to the possibility of inter-observer error	Objective in nature and permits semiquantitative measurement
Criteria for biomarker grading	Based on percentage of stained cells and stain intensity	SERS mapping based on average spectral intensity
HER2 receptor grading	2^+/Equivocal samples required FISH confirmation	By ratiometric semi quantitative approach FISH confirmation can be justified
Criteria	Cons of SERS over IHC	
	IHC	SERS
Instrument cost	Inexpensive bright field histopathology microscope	Expensive Raman microscope is required
Clinical validation	Clinically validated technique	Clinical validation yet to be done
High throughput analysis	Automated systems are available	Advancement in the technique is required
Requirement of artificial intelligence (AI)	Not required	With the support of AI method, the technique can be improved for quantitative detection.

the IHC staining pattern (Fig. 4 f).

2.5. Practical diagnostic applicability of RL-SERS-nanotags by large area SERS imaging

The major bottleneck of our multiplexed SERS analysis in tissue samples was to screen the entire area of the tissue specimen (usually of 5–10 mm^2 area) by Raman mapping since it generally allows visibility up to 0.15 mm^2–0.2 mm^2 area only in minimal time. To accomplish the total specimen analysis, large area Raman scanning technique was carried out with total areas covering 0.5 as well as 5 mm^2. Fig. S15 demonstrates the large area scanning with 0.5 mm^2 area of the duplexing analysis, which was performed in various combinations like ER/PR, PR/HER2 and ER/HER2 along with TNBC samples (Fig. S16). The results illustrate the large area scanning as a robust method to cover maximum tissue area to get more accuracy. Owing to the excellent sensitivity of the SERS-nanotags, we have achieved a large area scan of up to 5 mm^2, which provided a clear-cut idea about the prevalence of biomarkers in the sample. This method was able to accurately detect different biomarkers in combination from the scanning spectrum of gratifying resolution within 45 min scan duration (Figs. S17–S20). Considering the high throughput analysis of samples, still it is required to analyze many samples at that stipulated time, which can be addressed by the advancements of current technologies in future. A comparative analysis of conventional IHC and SERS techniques explaining the pros and cons of the both is summarized in Table 1.

3. Conclusion

In summary, we have successfully introduced RL-SERS-nanotags based diagnostic platform for the detection of clinically relevant breast cancer biomarkers in singleplex, duplex as well as triplex fashion of IHC-confirmed breast cancer tissue subtypes. Optimized analysis mode of the RL-SERS-nanotags along with untargeted isotype control SERS-nanotag rendered least non-specific binding and ensured to minimize the false positive results. Moreover, HER2 grading by ratiometric profiling of HER2 and isotype control tags eventually confirmed the 1^+, 2^+ and 4^+ tissue samples were perfectly complementing with time-consuming IHC as well as expensive FISH analysis. Finally, we have executed the whole area Raman mapping of a single specimen with the multiplexing RL-SERS tags reflecting the capability of the newly emerged platform to provide rapid results in less than an hour with minimal non-specific binding. The study thus reveals a robust and highly sensitive diagnostic modality with futuristic potential for the detection of tumors as well as tumor recurrence exhibiting differential biomarkers associated with patient-to-patient heterogeneity. The inability of the system to perform high throughput analysis in a fixed time may be improved by the introduction of advancements in instrumentation in near future.

4. Experimental section

Detailed methodology of nanoparticle synthesis, characterization, RR incorporation, antibody conjugation, biocompatibility analysis, tissue processing methods and SERS analysis parameters are provided in the supporting information.

CRediT authorship contribution statement

Vishnu Priya Murali: Methodology, Validation, Formal analysis, Investigation, Data curation, Writing – original draft, Writing – review & editing. **Varsha Karunakaran:** Methodology, Validation, Formal analysis, Investigation, Data curation, Writing – original draft, Writing – review & editing. **Madhukrishnan Murali:** Methodology, Formal analysis, Investigation. **Asha Lekshmi:** Methodology, Validation, Formal analysis, Investigation. **Shamna Kottarathil:** Methodology, Formal analysis, Investigation. **Selvakumar Deepika:** Methodology, Formal analysis, Investigation. **Valliamma N. Saritha:** Validation. **Adukkadan N. Ramya:** Investigation. **Kozhiparambil G. Raghu:** Supervision, Resources. **Kunjuraman Sujathan:** Conceptualization, Supervision, Methodology, Validation, Resources, Project administration. **Kaustabh Kumar Maiti:** Conceptualization, Methodology, Validation, Formal analysis, Writing – original draft, Writing – review & editing, Funding acquisition, Resources, Project administration.

Declaration of competing interest

The authors declare that they have no known competing financial interests or personal relationships that could have appeared to influence the work reported in this paper.

Data availability

Data will be made available on request.

Acknowledgements

Funding provided by CSIR Mission mode project, Nano-biosensor and Microfluidics for Healthcare (HCP-0012) to perform this study is gratefully accredited by K.K.M., K.S. V.P.M. thanks the CSIR mission mode project (HCP-0012), CSIR-FTT project, Customized Portable Raman spectrophotometric device for multiplex detection of breast cancer biomarkers (MLP-0039) and DHR Young Scientist program (R.12014/22/2021-HR/E-office:8114716). VK acknowledges ICMR-SRF for research fellowship, AcSIR Ph.D. student M.K.M thank UGC for research fellowship. D.S. and S.K. thanks the CSIR mission mode project, Nano-biosensor and Microfluidics for Healthcare (HCP-0012). A.L. acknowledges the CSIR mission mode project (HCP-0012) and DHR Young scientist program (R.12014/07/2021-HR/E-office:8114716), A.N.R

thanks CSIR-SRF for research fellowship. Authors are grateful to Dr Sudeep Gupta, Director, Advanced Centre for Treatment, Research and Education in Cancer (ACTREC), Tata Memorial Centre, Mumbai, India for the valuable suggestions and guidance. Author 1 and Author 2 contributed equally to this work.

Appendix A. Supplementary data

Supplementary data to this article can be found online at https://doi.org/10.1016/j.bios.2023.115177.

References

Bogdanovska-Todorovska, M., Kostadinova-Kunovska, S., Jovanovik, R., Krsteska, B., Kondov, G., Kondov, B., Petrushevska, G., 2018. Open access maced. J. Med. Sci. 6, 593–599.
Cornejo, K.M., Kandil, D., Khan, A., Cosar, E.F., 2014. Arch. Pathol. Lab Med. 138, 44–56.
Costa, R.L.B., Czerniecki, B.J., 2020. npj Breast Cancer 6, 10.
Davis, R.M., Kiss, B., Trivedi, D.R., Metzner, T.J., Liao, J.C., Gambhir, S.S., 2018. ACS Nano 12, 9669–9679.
Dinish, U.S., Balasundaram, G., Chang, Y.T., Olivo, M., 2014. J. Biophot. 7, 956–965.
Dixon, A.R., Bathany, C., Tsuei, M., White, J., Barald, K.F., Takayama, S., 2015. Expert Rev. Mol. Diagn. 15, 1171–1186.
Furrer, D., Sanschagrin, F., Jacob, S., Diorio, C., 2015. Am. J. Clin. Pathol. 144, 686–703.
Haka, A.S., Shafer-Peltier, K.E., Fitzmaurice, M., Crowe, J., Dasari, R.R., Feld, M.S., 2005. Proc. Natl. Acad. Sci. U.S.A. 102, 12371–12376.
Hernandez, S., Rojas, F., Laberiano, C., Lazcano, R., Wistuba, I., Parra, E.R., 2021. Front. Mol. Biosci. 8, 1–10.
Joseph, M.M., Narayanan, N., Nair, J.B., Karunakaran, V., Ramya, A.N., Sujai, P.T., Saranya, G., Arya, J.S., Vijayan, V.M., Maiti, K.K., 2018. Biomaterials 181, 140–181.
Lange, Carol A D.Y., 2008. J. Mol. Endocrinol. 4, 151–162.
Lee, S., Chon, H., Lee, J., Ko, J., Chung, B.H., Lim, D.W., Choo, J., 2014. Biosens. Bioelectron. 51, 238–243.
Li, M., Kang, J.W., Sukumar, S., Dasari, R.R., Barman, I., 2015. Chem. Sci. 6, 3906–3914.
Lin, C.Y., Yu, C.J., Lin, Y.H., Tseng, W.L., 2010. Anal. Chem. 82, 6830–6837.
Lin, D., Hsieh, C.L., Hsu, K.C., Liao, P.H., Qiu, S., Gong, T., Yong, K.T., Feng, S., Kong, K. V., 2021. Nat. Commun. 12, 3430.
Maiti, K.K., Dinish, U.S., Samanta, A., Vendrell, M., Soh, K.S., Park, S.J., Olivo, M., Chang, Y.T., 2012. Nano Today 7, 85–93.
Narayanan, N., Karunakaran, V., Paul, W., Venugopal, K., Sujathan, K., Kumar Maiti, K., 2015. Biosens. Bioelectron. 70, 145–152.
Nariman, B., Anne, F., Marie, H.J., Yubing, S., Byung, K., 2017. Nanotechnology 28, 455101.
Njoki, P.N., Lim, I.I.S., Mott, D., Park, H.Y., Khan, B., Mishra, S., Sujakumar, R., Luo, J., Zhong, C.J., 2007. J. Phys. Chem. C 111, 14664–14669.
Parise, C.A., Caggiano, V., 2014. J. Cancer Epidemiol., 469251, 2014.
Ramya, A.N., Arya, J.S., Madhukrishnan, M., Shamjith, S., Vidyalekshmi, M.S., Maiti, K. K., 2021. An Asian J 16, 409–422.
Ramya, A.N., Samanta, A., Nisha, N., Chang, Y.T., Maiti, K.K., 2015. Nanomedicine 10, 561–571.
Russo, J., Russo, I.H., 2006. J. Steroid Biochem. Mol. Biol. 102, 89–96.
Schlücker, S., Salehi, M., Bergner, G., Schütz, M., Ströbel, P., Marx, A., Petersen, I., Dietzek, B., Popp, J., 2011. Anal. Chem. 83, 7081–7085.
Shah, R., Rosso, K., David Nathanson, S., 2014. World J. Clin. Oncol. 5, 283–298.
Sheng, W., Zhang, C., Mohiuddin, T.M., Al-rawe, M., Zeppernick, F., Falcone, F.H., Meinhold-heerlein, I., Hussain, A.F., 2023. Int. J. Mol. Sci. 24, 3086.
Sun, J., Li, W., Zhu, X., Jiao, S., Chang, Y., Wang, S., Dai, S., Xu, R., Dou, M., Li, Q., Li, J., 2021. J. Agric. Food Chem. 69, 11494–11501.
Tan, W.C.C., Nerurkar, S.N., Cai, H.Y., Ng, H.H.M., Wu, D., Wee, Y.T.F., Lim, J.C.T., Yeong, J., Lim, T.K.H., 2020. Cancer Commun. 40, 135–153.
Wang, Y., Kang, S., Doerksen, J.D., Glaser, A.K., Liu, J.T.C., 2016. IEEE J. Sel. Top. Quant. Electron. 22, 6802911.
Wang, Y., Reder, N.P., Kang, S., Glaser, A.K., Yang, Q., Wall, M.A., Javid, S.H., Dintzis, S. M., Liu, J.T.C., 2017. Cancer Res. 77, 4506–4516.
Wang, Y. "Winston, Khan, A., Som, M., Wang, D., Chen, Y., Leigh, S.Y., Meza, D., McVeigh, P.Z., Wilson, B.C., Liu, J.T.C., 2014. Technology 118–132, 02.
Wang, Y., Yan, B., Chen, L., 2013. Chem. Rev. 113, 1391–1428.
Wang, Y.W., Doerksen, J.D., Kang, S., Walsh, D., Yang, Q., Hong, D., Liu, J.T.C., 2016. Small 12, 5612–5621.
Wesoła, M., Jeleń, M., 2015. Adv. Clin. Exp. Med. 24, 899–904.
Zavaleta, C.L., Garai, E., Liu, J.T.C., Sensarn, S., Mandella, M.J., Van De Sompel, D., Friedland, S., Van Dam, J., Contag, C.H., Gambhira, S.S., 2013. Proc. Natl. Acad. Sci. U.S.A. 110, E2288–E2297.

Nanomedicine: Nanotechnology, Biology, and Medicine
29 (2020) 102276

nanomedjournal.com

Diagnostic spectro-cytology revealing differential recognition of cervical cancer lesions by label-free surface enhanced Raman fingerprints and chemometrics☆

Varsha Karunakaran, MSc[a,c], Valliamma N. Saritha, PhD[d], Manu M. Joseph, PhD[a], Jyothi B Nair, PhD[a], Giridharan Saranya, MSc[a,c], Kozhiparambil G. Raghu, PhD[b,c], Kunjuraman Sujathan, PhD[d,*], Krishnannair S. Kumar, PhD[e,**], Kaustabh K. Maiti, PhD[a,c,***]

[a]*CSIR-National Institute for Interdisciplinary Science & Technology (NIIST), Chemical Sciences & Technology Division (CSTD), Organic Chemistry Section, Industrial Estate, Thiruvananthapuram, Kerala, India*

[b]*CSIR-National Institute for Interdisciplinary Science & Technology (NIIST), Agro-Processing and Technology Division (APTD), Industrial Estate, Thiruvananthapuram, Kerala, India.*

[c]*Academy of Scientific and Innovative Research (AcSIR), Ghaziabad, India*

[d]*Regional Cancer Centre (RCC), Division of Cancer Research, Thiruvananthapuram, Kerala, India*

[e]*Department of Future Studies, University of Kerala, Kariavattom, Kerala, India*

Revised 15 July 2020

Abstract

Herein we have stepped-up on a strategic spectroscopic modality by utilizing label free ultrasensitive surface enhanced Raman scattering (SERS) technique to generate a differential spectral fingerprint for the prediction of normal (NRML), high-grade intraepithelial lesion (HSIL) and cervical squamous cell carcinoma (CSCC) from exfoliated cell samples of cervix. Three different approaches i.e. single-cell, cell-pellet and extracted DNA from oncology clinic as confirmed by Pap test and HPV PCR were employed. Gold nanoparticles as the SERS substrate favored the increment of Raman intensity exhibited signature identity for Amide III/Nucleobases and carotenoid/glycogen respectively for establishing the empirical discrimination. Moreover, all the spectral invention was subjected to chemometrics including Support Vector Machine (SVM) which furnished an average diagnostic accuracy of 94%, 74% and 92% of the three grades. Combined SERS read-out and machine learning technique in field trial promises its potential to reduce the incidence in low resource countries.

Key words: Surface enhanced Raman spectroscopy; Cervix; Label-free; Gold nanoparticle; Human papilloma virus

Cervical cancer is the 4th common cancer in women worldwide leading to malignancy related death.[1] In India, the second most populous country in the world, cervical cancer accounts for 22.86% of all cancers among women. The incidence of this disease has been reduced dramatically by the implementation of screening programs in developed countries including a consolidated tactics inclusive of early detection, prevention, screening and proper treatment programs. The predisposing

The authors declare no competing financial interest.

Acknowledgments: K.K.M., K.S. and K.S.K. thank the CSIR Mission mode project Nanobiosensor and microfluidics for healthcare (HCP-0012) and 60 (0113)16/EMRII, Department of Science and Technology (DST) Nano Mission, Government of India (SR/NM/NS-1152/2016). K.K.M. and J.B.N. are grateful to the Department of Biotechnology (DBT), Government of India (No. BT/ PR26670/NNT/28/1367/2017) for research funding. AcSIR Ph.D. students V.K. and G.S. thank I.C.M.R. and U.G.C. respectively for research fellowship. M.M.J. thanks the Science & Engineering Research Board (SERB), Department of Science and Technology, Government of India for the National Post-Doctoral Research Fellowship (PDF/2016/001391).

*Correspondence to: K. Sujathan, Regional Cancer Centre (RCC), Division of Cancer Research, Medical College PO, Thiruvananthapuram 695011, Kerala, India.

**Correspondence to: K.S. Kumar, Department of Futures Studies, University of Kerala, Kariavattom, Thiruvananthapuram, Kerala, India, 695 581.

***Correspondence to: K.K. Maiti, AcSIR, Chemical Sciences and Technology Division, CSIR- National Institute for Interdisciplinary Science and Technology (NIIST), Industrial Estate PO, Pappanamcode, Thiruvananthapuram, India, 695019.

E-mail addresses: sujathan@rcctvm.gov.in, (K. Sujathan), kskumar@keralauniversity.ac.in, (K.S. Kumar), kkmaiti@niistres.in. (K.K. Maiti).

https://doi.org/10.1016/j.nano.2020.102276
1549-9634/

factor for the cause of cervical cancer is the persistent infection with high risk human papilloma virus (HPV).[2] The Bethesda system refers different stages of cervical dysplasia which can be identified by a Pap smear test,[3] a well-established cytological staining technique practiced in clinics for identifying cancerous lesions by gently collecting exfoliated cells from the cervix. The chronological occurrence of epithelial abnormalities leads to the development of invasive cancer starting from healthy to low grade squamous intraepithelial lesion (LSIL/ CINI/ mild dysplasia), then to high grade squamous intraepithelial lesion (HSIL/ CIN II & III / moderate) and finally to invasive squamous cell carcinoma (severe dysplasia/ in situ carcinoma).[4] Even though Pap staining is a well-established routine test, some recent reports suggest its limitations owing to low sensitivity, high false negative rates, and inter-observer variability. The sensitivity was found to be 51% only with 98% specificity and 35.5% false negative rate.[5,6] These limitations have forced to re-evaluate the significance of cytology as a primary screening test. HPV DNA analysis has also been included in the cervical cancer detection strategy using polymerase chain reaction (PCR), but many of the HPV infections are transient without causing any clinically significant lesions and get cleared without any intervention, upon time. Hence, the specificity and positive predictive value of HPV test in a population is considerably low. Therefore, Pap smear plus HPV testing and vaccination against high risk HPV is considered as a forefront overall strategy for the effective control of cervical cancer in developed countries. Lack of adequate trained manpower[7] to screen all eligible women in the community is an additional impediment for implementing such population screening programs in a systematic manner. Therefore, there is an urgent need for low cost alternative techniques which should ideally be rapid, non-destructive and objective to emerge as a population screening program.

A molecular level study of cellular and biological processes are essential for understanding the mechanism and detection of diseases together with its therapeutic outcomes. The quest for specific and accurate cancer screening has driven the development of novel diagnostic methods including spectroscopic techniques to improve detection of target biomarkers, especially to distinguish early malignant lesions.[8] Non-invasive diagnosis of malignancies has been well-studied by optical spectroscopic methods, mostly by Fourier-transform infrared spectroscopy,[9] Raman[10] fluorescence[11] etc. and out of which Raman spectroscopy offers some distinctive benefits over other techniques. It is based on inelastic scattering of monochromatic light possessing high spatial resolution which can pretend near-infrared (NIR) radiation with less sample preparation and minimal influence of water bands. A large number of studies employing Raman scattering together with an accurate database for each characteristic peak frequencies to analyze non-cancerous or cancerous tissues,[12] classification of normal, malignant and benign samples for different cancers like breast,[13] cervical[14] oral,[15] gastric[16] etc. using various multivariate analysis[17] has been developed. The challenges associated with large data sets has been resolved extensively by applying various chemometric methods,[18] such as principal component analysis (PCA),[19] linear discriminant analysis (LDA),[20] least-squares regression as well as cluster analysis and machine learning techniques like Support Vector Machine (SVM).[21] However, a major issue of Raman scattering is its inherently weak signal which led to a handful of improvisations over typical Raman spectroscopy out of which Surface Enhanced Raman Scattering (SERS),[22,23] received huge acceptance allowing the ultrasensitive detection of analytes with low concentration through the amplified signals around 10^8–10^{14} folds by the excitation of surface plasmons rendered by metallic nanoparticles. The potential of ultrasensitive SERS analysis in single living cells has been demonstrated using colloidal gold nano particles (AuNPs) deposited inside cells which resulted in strong enhancement of Raman signals of biomolecules opening up exciting opportunities for biomedical studies.[24] Subsequently, several studies based on SERS platform was explored including the precise tracking of the biomolecular changes in different stages of mitosis,[25] apoptosis,[26] classification of healthy and cancerous samples in breast cancer,[27] bladder cancer,[28] gastric cancer,[29] colorectal cancer[30] parotid cancer,[31] kidney tumor staging[32] etc.

Cervical cancer has been well studied by conventional Raman spectroscopy in the past several years for differentiating normal and abnormal subjects using blood serum,[33] cells,[34–36] tissues,[37] in vivo[38] etc. When compared to the conventional Raman spectroscopy, SERS is an ultrasensitive technique requiring very less acquisition time, better signal to noise ratio, increased fold intensity, specificity and Raman cross section. A few SERS studies on cervical cancer has been reported using blood plasma-[39] and serum[40] samples but all these cases involves invasive sample collection procedures. Also, blood based biomolecular changes like leakage of circulating tumor cells, DNA, proteins, exosomes etc. will be prevalent in the metastatic stage only, so early stage detection or classification using blood is not practicable. However, employing SERS in exfoliated cell samples for cervical cancer detection will provide direct insight into the origin of abnormality. Considering the existing diagnostic modalities and upcoming fundamental issues, we report for the first time, a label free SERS based spectroscopic approach in exfoliated cells for generating a sensitive differential spectral fingerprint for straight forward detection of squamous cell carcinoma and its precursor lesions during the progression of cervical cancer. The analysis has been performed for distinguishing three groups i.e. NRML, HSIL and CSCC using three different forms of analytes viz. single cell, cell-pellet, extracted DNA (Figure 1). Significant peak variations, shifts and spectral differences were evaluated within and between the groups using chemometric interpretation viz., PCA, LDA and SVM in order to generate the prediction accuracy showing its potential to emerge as a screening method to monitor the progression of cervical cancer. Along with SERS based spectro-cytology as a new insight, comparative conventional cytological and HPV PCR analysis were also carried out. Another hallmark of cancer progression is the altered metabolism to satisfy the increasing need of energy. Intracellular concentration of amino acids is a diagnostic parameter for cancer as the abnormal proliferation requires more amino acids for protein synthesis. Thus, amino acid profiling by ultra-fast liquid chromatography (UFLC) technique[41] was attempted as an alternative confirmatory approach for identifying the progression of cancer related amino acid metabolites along with SERS.

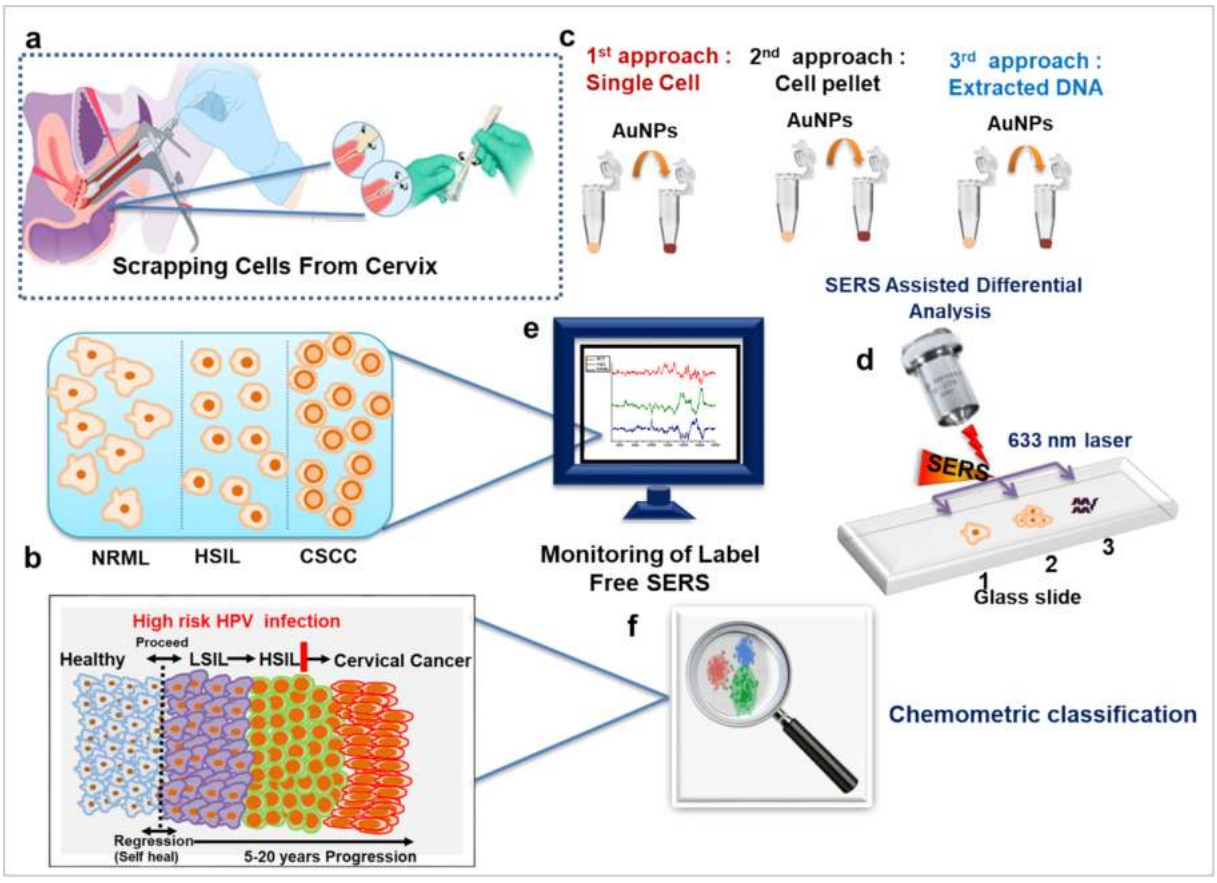

Figure 1. Schematic illustration of experimental design for differentiating three grades viz. normal (NRML), high grade intraepithelial lesion (HSIL), cervical squamous cell carcinoma (CSCC) using SERS., a) Scrapping cells from the cervix using cytobrush, b) progression pattern of cervical cancer c) Set 1: single cell, Set 2: cell pellet, Set 3: extracted DNA (mixed with AuNPs), d) independent SERS analysis of 1) single cell,2) cell pellet, 3) extracted DNA in glass slide, d) empirical signal monitoring of the three grades f) chemometric analysis.

Methods

Chemicals and materials

Gold (III) chloride hydrate, trisodium citrate dehydrate were purchased from Sigma-Aldrich. Ethyl alcohol (99.9% purity) was purchased from Changshu Yangyuan Chemical, China. Detailed description of experiments is provided in the supporting information.

SERS substrate preparation

Gold nanoparticles (AuNPs, 40–45 nm) were synthesized by well-known citrate reduction method.

SERS analysis and data analysis

Spectral analysis using confocal Raman analysis was performed with the aid of a confocal Raman microscope (WITec, Inc., Germany, alpha 300R) with a laser beam directed to the sample through 20× objective with a Peltier cooled CCD detector. Detailed procedure is provided in the supporting information. The raw spectral data were pre-processed by Project FOUR 4.0 (WITec, Germany) before the data statistical analysis in order to remove the interference noises, cosmic rays and oversaturated spectra. PCA, LDA and SVM statistical chemometric tools were utilized for the classification.

Results

Fabrication of colloidal SERS substrate

We have employed colloidal spherical AuNPs (absorbance 530 nm) within a size range of 40–45 nm emphasizing its best SERS activity[42,43] reported so far. AuNPs synthesized as per the standard method[44] with optimized size, shape and monodispersity were confirmed by Ultraviolet–visible (UV–Vis) absorbance, Dynamic Light Scattering (DLS) and High Resolution Transmission Electron Microscopy (HR-TEM) (**Supplementary Figure S1**). Colloidal AuNPs concentrations were obtained nearly 8–10 × 10^{10} particles/ml.

Biomolecular fingerprinting of cervical squamous cell carcinoma model

Label-free biomolecular SERS fingerprints were evaluated with an epithelial type cell line, SiHa derived from grade II squamous cell carcinoma of the cervix which can be considered

as the best in vitro model prior to clinical investigation. SERS analysis showed the presence of a range of molecular fingerprints out of which Raman peaks at 481, 1330 and 1456 cm^{-1} corresponds to the -C-N-C-bending, -P=O-stretching vibration and -CH2 vibration of DNA signal, 572 cm^{-1} designates the -O-C=O for tryptophan abundance, 621 and 1002 cm^{-1} relates to signals from -O-C=O and aromatic ring chain vibration in phenyl alanine, 643 and 1211 cm^{-1} represents -O-C=O bending and -C-C-N- vibration in tyrosine, 735 and 746 cm^{-1} represents -O-C=O bending vibration in adenine and thymine respectively (**Supplementary Figure S2**). We also observed Raman peaks at 826 and 1085 cm^{-1} corresponds to DNA phosphate backbone (-O-P-O-) stretching vibration, 957 and 1154 cm^{-1} indicated the presence of -C-C- aliphatic alicyclic chain vibration in carotenoids and peak at 1545 cm^{-1} resembled the presence of Amide II, nucleic acid and tryptophan, 1697 cm^{-1} corresponds to Amide I (**Supplementary Table S1**).[12] The distinct well resolved biomolecular fingerprints from SiHa cells provided a blue-print of the major molecular fingerprint viz., aromatic amino acid, DNA, Amides (I & II), which were benchmarked as a model for clinical investigations.

SERS-aided grading with cervical exfoliated single cells

Pathologically confirmed cervical smears of major three grades i.e. NRML, HSIL and CSCC were processed using liquid based cytology procedure. The details of patient samples is depicted in **Supplementary Table S2**. A monolayer of diagnostically relevant cells upon incubation with AuNPs was evaluated for the single cell analysis. In a preliminary analysis, the SERS mapping of the single cell showed the variations in the morphology of three different types of cells, viz. NRML, HSIL and CSCC (Figure 2, *a*). In single cells, 5 μm × 5 μm nuclear area was preferred for image scanning to avoid variability arising from the cytoplasmic area. Since the analysis involved addition of AuNPs, Pap stained slides were subjected to de-staining followed by SERS analysis to select the diagnostically relevant cells (**Supplementary Figure S3**).

Initially, individual SERS fingerprint was evaluated empirically followed by chemometric statistical analysis to group the three classes. The mean spectra accumulated from the average of the collected spectrum excluding the outliers were normalized to its highest peak (Amide II at 1550 cm^{-1}) for observing the spectral variations. The analysis in exfoliated single cell samples,

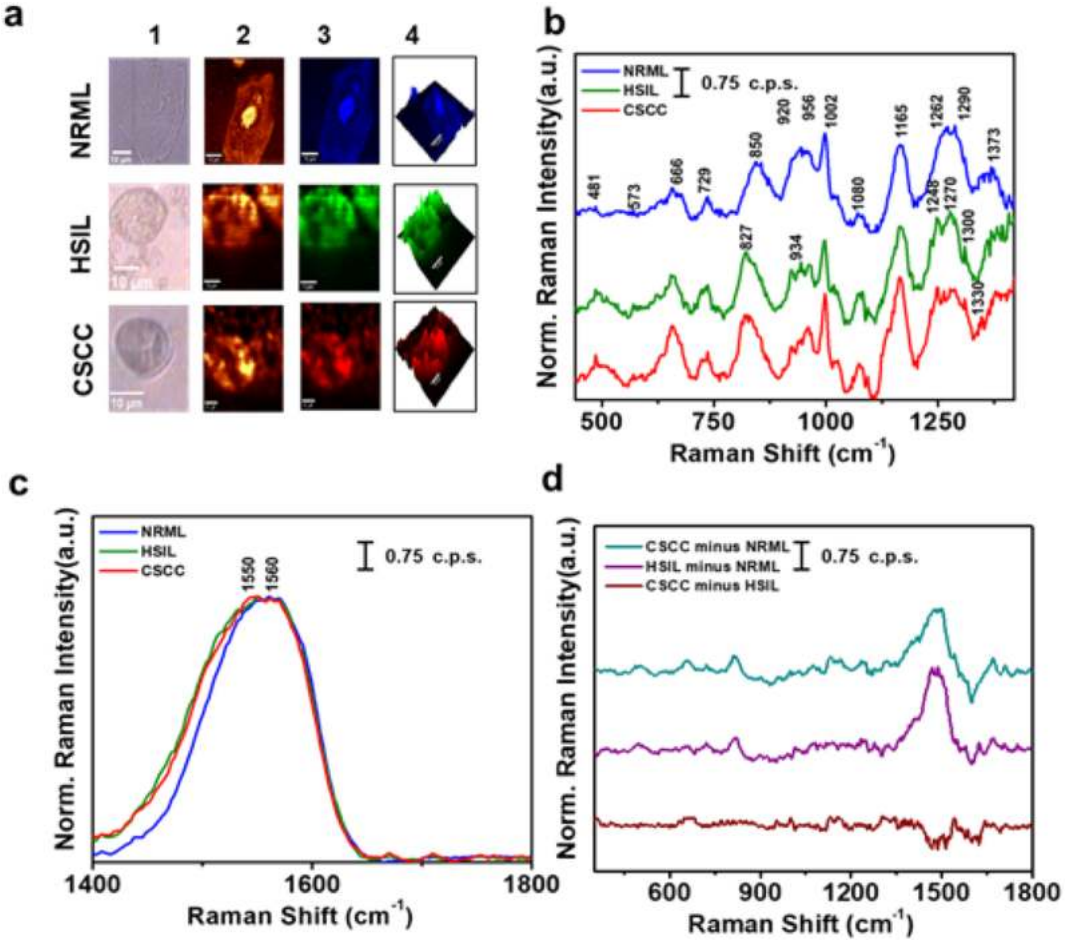

Figure 2. SERS analysis from exfoliated single cell samples**,** a) SERS imaging of single cell, 1) Bright field, 2) Raman imaging, 3) cluster mapping and 4) 3D cluster mapping (Scale bar: 10 μm, Laser power density 3–7 mW power density), b) Mean SERS spectra acquired from cervical exfoliated single cell samples (region 400–1400 cm^{-1}), c) Mean SERS spectra from range 1400–1800 cm^{-1}, d) Difference SERS spectra for NRML, HSIL and CSCC samples.

NRML, HSIL and CSCC showed distinctive peaks correlating to the model cell line signals. Distinct Raman peak at 481 cm^{-1} associated with -C-N-C bending vibration of DNA was found to be increased in HSIL and CSCC samples which showed an indication of high nuclear content. The -O-C=O- bending vibration of amino acid tryptophan corresponding to 573 cm^{-1} was prominent in HSIL and CSCC samples displaying the presence of high protein content which may be mostly from the histone protein and nuclear regulatory proteins inside the nucleus. The -O-C=O- bending vibration peak at 643 and 666 cm^{-1} are indicative to tyrosine, thymine and guanine ring vibrations present in all grades whereas adenine ring vibration at 729 cm^{-1} identified prominently in the abnormal grades i.e. HSIL and CSCC predicting the increase in nuclear elements. On the other hand, O-P-O stretching at 826 cm^{-1} and 1080 cm^{-1} favored the indirect existence of nucleic acid. A -C-O-C- bending vibration peak at 920 cm^{-1} is slightly prominent in abnormal samples which correspond to the amino acid, proline. C-C aliphatic, alicyclic peaks identified at 956 and 1165 cm^{-1} attributed to carotenoid showed higher intensity in CSCC compared with NRML. Amide III signal from proteins at 1262 cm^{-1} in NRML is shifted in HSIL and CSCC samples to 1270 cm^{-1}. Similarly, amide II signal arising at 1560 cm^{-1} from the protein counterparts inside the nucleus showed a clear shift of around 10 nm between normal and abnormal samples (Figure 2, *b* and *c*).[12] Interestingly, the ratio between 1270 and -O-C=O symmetric stretching at 1373 cm^{-1} were well resolved for the prediction of abnormality from the mean spectra. The ratio value was found to be 1.55, 1.2 and 1.02 for NRML, HSIL and CSCC respectively in single cells. The ratio is decreasing because the peak corresponding to 1373 cm^{-1} is increasing in the abnormal samples. The variations existing between the three groups were acquired by subtracting the mean spectra of NRML from CSCC, NRML from HSIL and HSIL from CSCC. The positive peaks in the difference spectra obtained showed the presence of bio-molecular activity and negative peaks showed the absence of the same (Figure 2, *d*). The differentiating peak were visualized by box plot analysis performed in R software (**Supplementary Figure S4**). All the peak assignments from the single cell analysis is depicted in **Supplementary Table S3**.

SERS-aided grading with cervical exfoliated cell pellets

In the pellet form of exfoliated cells, it exhibited a prominent SERS peak representing -C-O-C bending vibration at 490 and 1022 cm^{-1} corresponding to the presence of glycogen prevalent in NRML cells compare to abnormal cells in cervical smears. Identified -O-C=O Raman peaks at 667, 729 and 1373 cm^{-1} indicated the increase in the DNA material in HSIL, CSCC samples specific to thymine, guanine and adenine respectively. Again, sharp peak showing -C-C-N- at 1170 cm^{-1} corresponding to tyrosine was found in abnormal samples. Visible Raman peak shift was obtained at the Amide II region in the CSCC samples when compared to NRML samples as specified a peak at around 1568 cm^{-1} in NRML shifted to 1547 cm^{-1} in CSCC specimen (Figure 3, *a* and *b*). We have evaluated the ratio between P-O-C anti symmetric stretch at 970 and 1022 cm^{-1} which is considered as a predictive indicator of abnormality from the mean spectra leading to the values of 0.61, 1.13 and 1.34 for NRML, HSIL and CSCC respectively. The pellet comprising cervical exfoliated cells was a mixture of normal and abnormal cells with its mean signature Raman spectra contained some common features.

The variations existing between the three groups were attained by subtracting NRML from CSCC, NRML from HSIL and HSIL from CSCC mean spectra. The positive peaks in the difference spectra illustrated the presence of bio-molecular activity and negative peaks showed the absence of its fingerprints (Figure 3, *c*). Standard deviation and mean spectra is shown in Figure 3, *d*. The prominent peak differences between NRML, HSIL and CSCC samples were visualized in box plot analysis performed in statistical R software (**Supplementary Figure S5**). All the peak assignments from the cell pellet analysis is depicted in **Supplementary Table S4**.

SERS-aided grading with cervical exfoliated cell DNA

In the progression of Raman fingerprinting obtained from single cell and cell pellet analysis for the differential diagnosis of cervical precancerous and cancerous lesions, cellular DNA was extracted to re-investigate nucleotide profiling. Majority of the SERS peaks obtained from extracted DNA correlated with the peaks obtained from the single cell and cell pellet. The specific peaks at 729 cm^{-1} corresponded to -O-C=O- adenine ring vibration, 826 and 1080 cm^{-1} related to the O-P-O stretching vibration in DNA, 1172 cm^{-1} attributed to -C-C-N- bending vibration in cytosine and guanine, 1421 and 1578 cm^{-1} were related to -C-N- stretching vibration and NH_2 deformation in Amide II in adenine and guanine (Figure 4, *a*). Difference spectra were assessed by subtracting NRML from CSCC, NRML from HSIL and HSIL from CSCC mean spectra from the DNA samples (Figure 4, *b*). The mean spectra and standard deviation is shown in Figure 4, *c*. The peak variations significant between NRML, HSIL and CSCC DNA samples were measured in box plot analysis employing R software (**Supplementary Figure S6**). All the peak assignments from the extracted DNA analysis is depicted in Figure 4, *d*.

UFLC analysis of amino acid metabolites in cervical exfoliated cells

In the course of complementary validation, we have investigated the presence of amino acids contributing to the differential spectra obtained from single cell and cell pellet analysis by UFLC. A peak at retention time of 13.65 min in HSIL and CSCC samples were exactly correlating with the standard amino acid tryptophan. Similarly, the retention times of 15.45 min for tyrosine, 17.8 min for proline, and 18.6 min for phenyl alanine were identified in HSIL and CSCC with their respective standards. Interestingly, all the four amino acid peaks were negligible in NRML samples **(Supplementary Figure S7).** The presence of tyrosine, phenyl alanine, tryptophan and proline reflected in the progression stage in HSIL and CSCC samples leading to the increased protein content.

Chemometric analysis

As we obtained a large spectral data set in all the three groups NRML, HSIL and CSCC modeling and prediction of the same was very much essential to discriminate between them. Initially, we adopted chemometric analysis using PCA to

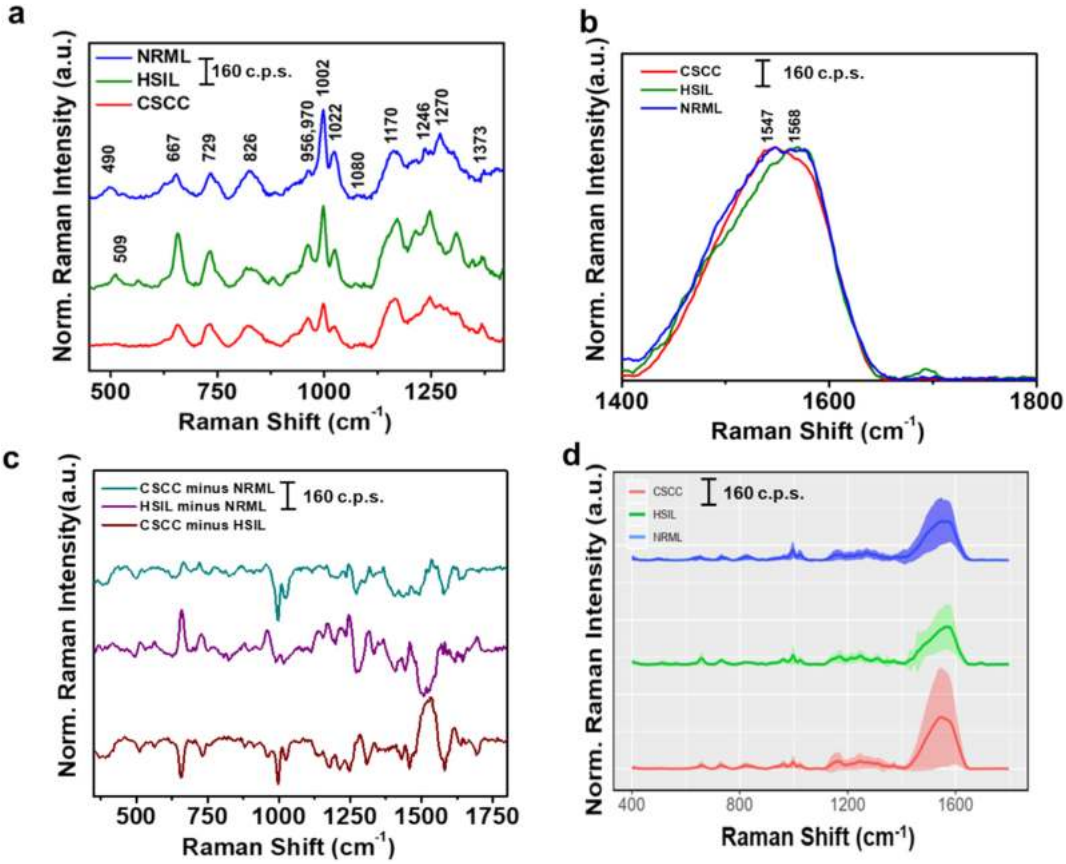

Figure 3. SERS analysis from exfoliated cell pellet samples, a) Mean SERS spectra acquired from cervical exfoliated cell pellet (region 400–1400 cm^{-1}), [Laser power density 3–7 mW power density], b) Mean SERS spectra of cell pellet from range 1400–1800 cm^{-1}, c) Difference SERS spectra, d) Tentative SERS peak assignments from cervical cell pellet samples; NRML, HSIL and CSCC.

classify them using MATLAB software. A predictive classification was obtained using PCA analysis in single cell, cell pellet and extracted DNA respectively (Figure 5, *a*, *c* and *e*). It was observed that the increase of noise in Raman spectra using PCA. Subsequently, the intra-group variability was enhanced which reflected to the reduction of specificity in PCA. Therefore, to improve the specificity we adopted LDA analysis as the next trial. LDA is a stereotype of Fisher's linear discriminate used in statistics, machine learning and pattern recognition into linear combination of features that characterizes or separates two or more classes and attempts to amplify the difference between the classes of data which is difficult to get from PCA. We observed a clear demarcation between single cell, cell pellet and extracted DNA from LDA analysis (Figure 5, *b*, *d*, and *f*). In the course of gradual improvement of prediction accuracy, SVM analysis was attempted by randomly selecting 75% of the spectra as the train set and rest 25% were used as the test set. The SVM analysis was repeated with 500 different random samples and measured the average prediction accuracy. The accuracy was found to be 94% for single cell, 74% for cell pellet and 92% for extracted DNA with 0.73%, 5.04% and 3.84% standard deviation respectively (Figure 6, *a–c*). Thus based on the created reference spectral module an unknown sample can be predicted. The percentage of prediction accuracy was generated along with ROC curve (Figure 6, *d–f*). ROC curve is a graphical plot which shows the diagnostic ability of a classifier system by varying the discrimination threshold. At different threshold setting, the ROC curve is plotted by true positive rate against false positive rate. True positive is termed sensitivity and false negative is termed 1-specificity. The accuracy of the analysis depends on how good the test separates the group got tested into those with and without the disease. Accuracy is measured by calculating the area under the curve. The ROC curve of single cell, cell pellet and extracted DNA showed that SVM is an incremental diagnostic model for classifying the groups (Figure 6, *g–i*). The sensitivity and prediction accuracy of the technique was calculated (Table 1).

Cytopathological Pap staining analysis

In order to get a clear discrimination between normal vs abnormal exfoliated cells, both bright field images from Raman microscope and Pap staining of NRML, HSIL and CSCC were evaluated for morphological analysis (Figure 7, *a* and *b*). All the abnormal samples were further confirmed by colposcopic biopsy. In Pap staining, the superficial NRML cells were stained pink with pyknotic nucleus, intermediate cells stained light blue

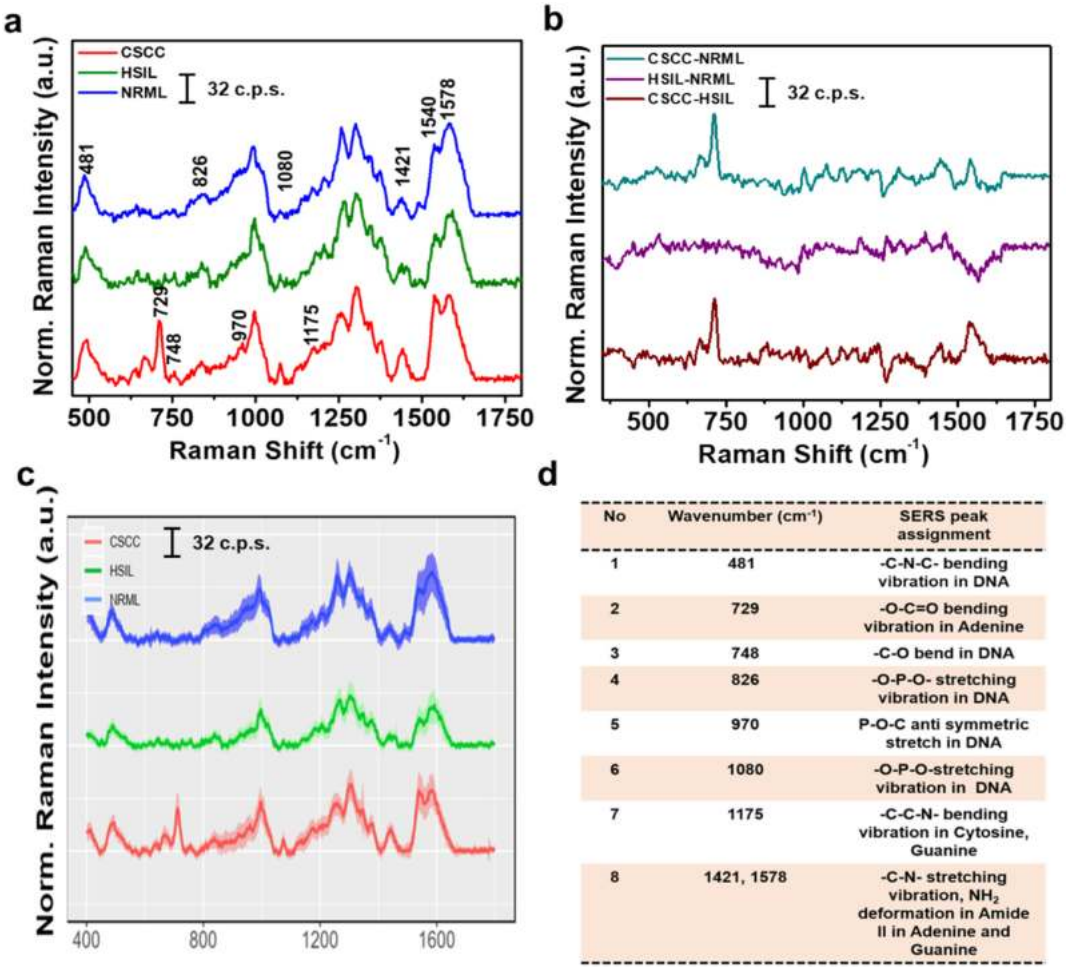

No	Wavenumber (cm^{-1})	SERS peak assignment
1	481	-C-N-C- bending vibration in DNA
2	729	-O-C=O bending vibration in Adenine
3	748	-C-O bend in DNA
4	826	-O-P-O- stretching vibration in DNA
5	970	P-O-C anti symmetric stretch in DNA
6	1080	-O-P-O-stretching vibration in DNA
7	1175	-C-C-N- bending vibration in Cytosine, Guanine
8	1421, 1578	-C-N- stretching vibration, NH_2 deformation in Amide II in Adenine and Guanine

Figure 4. SERS analysis from extracted DNA samples from exfoliated cells**,** a) Mean SERS spectra [Laser power density 3–7 mW power density], b) the difference spectrum, c) the standard deviation and d) tentative SERS peak assignments from cervical clinical DNA samples; NRML, HSIL and CSCC**.**

to green color where as in HSIL, the enlarged nucleus reflecting high DNA content with minimal cytoplasm showed purple color nucleus. In CSCC, the cells started to show invasive nature with a slender shape formation to the nucleus. To correctly identify the desired classes of cells, initially the Pap staining was performed to mark the cell position and the same cells were subjected to SERS analysis (**Figure S3**).

Human papillomavirus analysis

To identify the HPV specific DNA integrated in the infected samples, HPV PCR were employed. To evaluate and compare the Pap smear test, NRML, HSIL and CSCC samples were loaded after DNA isolation from the respective samples out of which HSIL and CSCC showed a band corresponding to HPV DNA. A PCR amplification product of size varying between 230 and 270 bp was obtained in 1.5% agarose gel indicative of an infection with oncogenic HPV in HSIL and CSCC whereas no observable band was identified for NRML samples (Figure 7, *c* and *d*). The PCR product obtained was indicative of oncogenic HPV types 16, 18, 31, 33, 35, 45, 52 and 58.

Discussion

As cervical cancer progresses from normal to abnormal in a grade dependent way, the identification of precancerous lesions can be beneficial for the early diagnosis. We have utilized AuNPs which is a well explored SERS substrate with tunable optical property and is chemically inert when mixed with a wide range of analytes or biomolecules providing characteristic Raman fingerprints. The analysis has been approached by the modulation of three different samples i.e. single cell, cell pellet and extracted DNA to arrive at a conclusion for adopting the most simplest and accurate results to uplift the technique as a diagnostic modality. Liquid based cytology (LBC) fixation were performed which improved preservation of the cell sample eliminating artifacts and degenerative changes developed in the course of air-drying. In addition, LBC will reduce the background caused by blood contamination in the cervical scrape samples which usually interferes in the sample interpretation.[45] SERS substrate incubation in fixed cells and living cells are the two widely used methods to study single cells using SERS. Reports suggests that valuable information of real

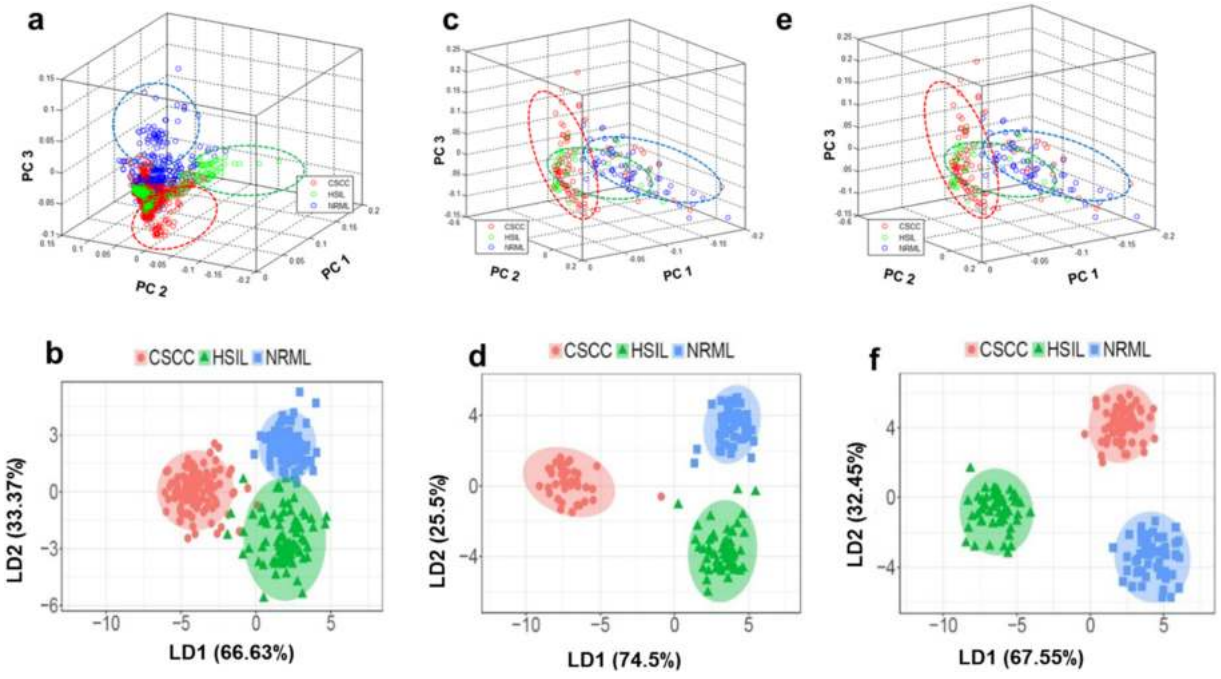

Figure 5. Chemometric discrimination between PCA and LDA scatter plots: (a, b) single cell, (c, d) pellet and (e, f) extracted DNA.

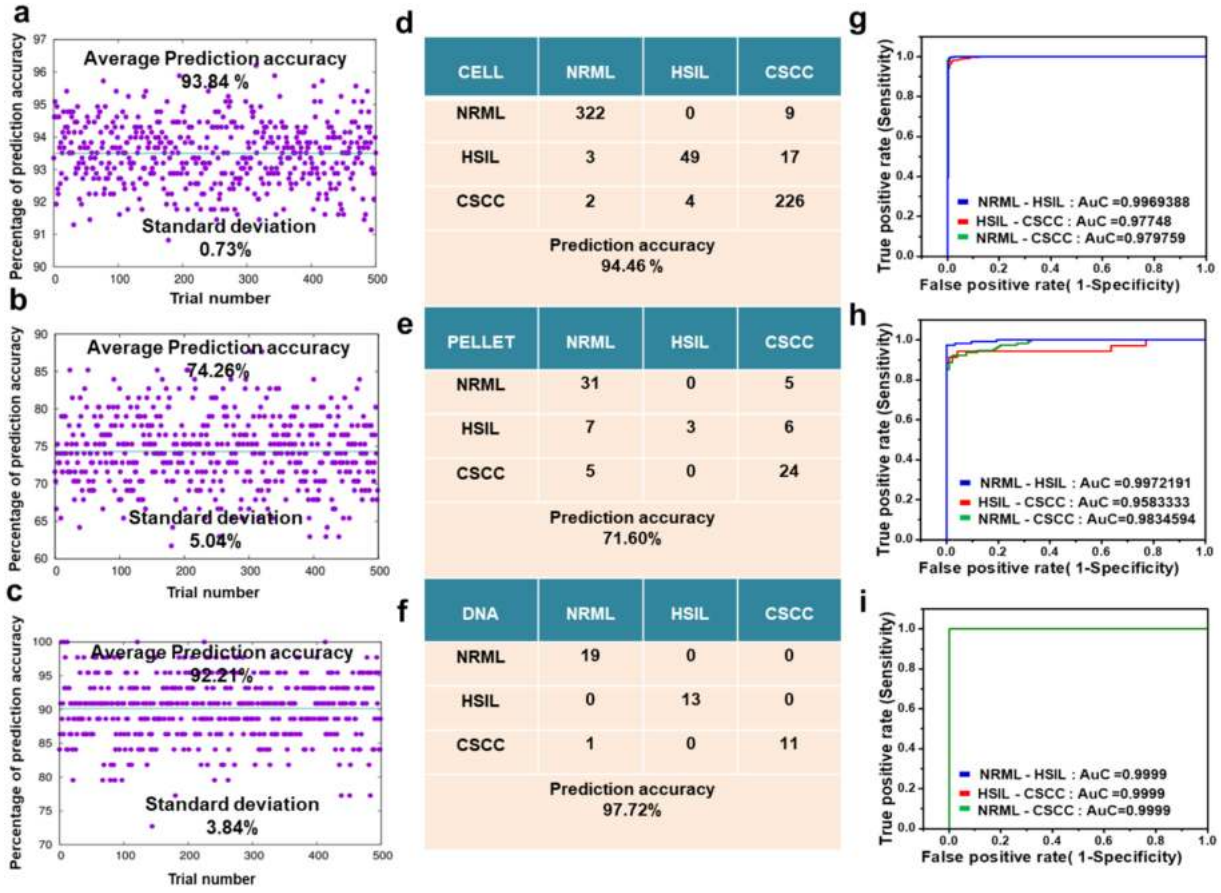

CELL	NRML	HSIL	CSCC
NRML	322	0	9
HSIL	3	49	17
CSCC	2	4	226

Prediction accuracy
94.46 %

PELLET	NRML	HSIL	CSCC
NRML	31	0	5
HSIL	7	3	6
CSCC	5	0	24

Prediction accuracy
71.60%

DNA	NRML	HSIL	CSCC
NRML	19	0	0
HSIL	0	13	0
CSCC	1	0	11

Prediction accuracy
97.72%

Figure 6. Percentage of average prediction accuracy chart in a) single cell, b) cell pellet and c) extracted DNA, Representative classification based on SVM analysis of d) single cell, e) cell pellet and f) extracted DNA, SVM ROC curve in g) cell, h) pellet and i) DNA.

Table 1
Sensitivity and prediction accuracy of SERS-based cervical precancerous lesions detection.

	Sample	Total	True prediction	False prediction	Prediction accuracy
Single cell	NRML	331	322/331	9/331	94.46% ± 0.73
	HSIL	69	49/69	20/69	
	CSCC	232	226/232	6/232	
Cell pellet	NRML	36	31/36	5/36	71.60% ± 5.04
	HSIL	16	3/16	13/25	
	CSCC	29	24/29	5/29	
Extracted DNA	NRML	19	19/19	0/19	97.72% ± 3.84
	HSIL	13	13/13	0/13	
	CSCC	12	11/12	1/12	

time cellular processes is obtained from live cells than fixed cells as fixation can lead to changes in the molecular vibrations leading to variations in the spectral pattern.[46] Our group has already demonstrated the accurate evaluation of surface charge of AuNPs for live cell uptake using positive, negative and neutral nanoparticles.[47] In the present study, as the cervical scrape cells are already fixed during collection, the variations thus arising is commonly assessed during the differential spectral evaluation in all the three groups, i.e. NRML, HSIL and CSCC spectra and finally such variations can be nullified.

Single cells were analyzed after morphologically identifying the ratio of nucleus to cytoplasm features. Cell pellet analysis were performed in a blinded manner without any morphological evaluation of the cells which may be the most ideal option for conducting a screening study. Extracted DNA analysis were performed to confirm the identity of Raman fingerprints of nucleic acids and UFLC analysis to profile the differential amino acids in the cervical cancer progression. The preliminary studies conducted in fixed SiHa cell line showed fingerprint peaks corresponding to amino acids, nucleic acid bases, phosphate stretchings, carotenoids etc. which formed a basis for the peak analysis in real patient samples. The O-P-O stretching at 826 cm^{-1} showed the increased nuclear content in HSIL and CSCC samples, which is identified as a shifted position in normal at 850 cm^{-1}. Such a peak shift is visible in IR-FT Raman spectra in cancerous cervix comparing benign and normal.[48] Another distinguishing factor between the three groups were the presence of -C-O-C- stretching of the amino acid proline.

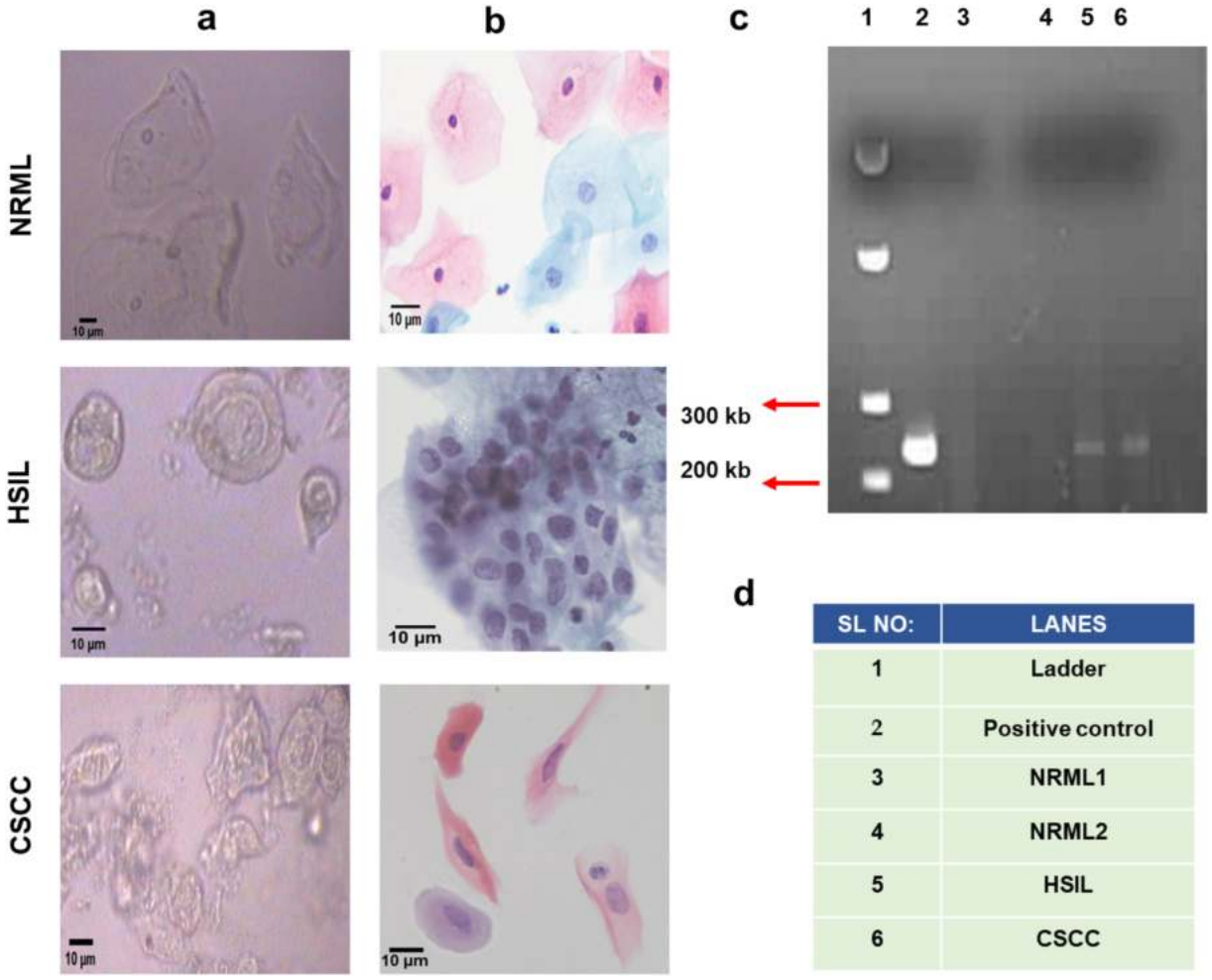

Figure 7. Conventional clinical cytopathological analysis of cervical exfoliated cells, a) Bright field and b) Pap stained images of NRML, HSIL and CSCC exfoliated cells, Scale bar corresponds to 10 µm, c) HPV PCR of clinical DNA samples and d) Sample loading order of HPV PCR ladder (1), positive control (2), NRML1 (3), NRML2 (4), HSIL(5), CSCC(6).

It has been proven that proline rich tyrosine kinase 2 (Pyk2) plays an important role in tumor progression in various human cancers.[49] Pyk2 is a non-receptor tyrosine kinase which controls tumor survival, its proliferation, migration, invasion properties, metastasis and resistance to chemotherapy.[50,51] In addition, there exists a correlation of a biomarker known as c-myc over expression distinct in cervical cancer which increases proline biosynthesis from glutamine and is a prognostic marker useful in guiding treatment decisions in cervical cancer. Pyk2 is also found to be essential for the intracellular trafficking of HPV 16 in human keratinocyte cells.[52–54] Thus the increase in proline may be indicative of tumor progression. The increase of carotenoid signal at 956 cm^{-1} and 1165 cm^{-1} in single cells might be due to the reason that cancer cells tends to accumulate carotenoids to resist damage.[55] Considering cell pellet, in positive sample it is said to be heterogeneous, i.e., all the three types of cells; viz. NRML, HSIL and CSCC may be present. Even though all cell types are present, there occurs a presence of premalignant changes in the normal looking cells[36] of the positive smears. The presence of glycogen is usually considered as a parameter for classifying normal and abnormal cells in cytological specimens of the cervix.[56,57] Extracted DNA analysis were performed to re-confirm the signals obtained from single cell and pellet sample analysis. Increase in DNA content was evident between the groups when compared with normal counterparts. For confirming the presence of amino acids playing differentially between the three classes, UFLC analysis were performed. The analysis confirmed the results obtained in SERS analysis by signals obtained from amino acids, tryptophan, tyrosine, phenyl alanine and proline. In addition to the real positive patient samples, SiHa cell also showed the presence of the above mentioned amino acids. As SiHa contains 1–2 copies[58] of HPV 16 and since Pyk2 is essential for the intracellular trafficking of HPV 16 in human keratinocyte cells, increase in proline may be the indicative for the tumor progression as mentioned earlier. Also, it is evident that cancer cells require more metabolic requirements for uncontrolled proliferation when compared to normal cells which is assessed by the specific amino acids for the metabolic reprogramming resulting in the deregulated replication. Chemometry was further utilized for the classification and prediction within the dataset employed for extracting data or information comprising complex data set from a chemical or biological source based on multivariate analysis, mathematical or computational models, to find the relationship between two or more closely related entities, structural analysis etc. PCA, LDA and SVM were performed out of which SVM showed good classification between the classes. The main advantage of PCA technique enabled to reduce the huge dimension of data-set without losing much information. But as the specificity was less, LDA and SVM analysis was attempted which increased the classification much better. Conventional analysis like Pap smear were performed to correctly identify the desired cells for SERS analysis. HPV PCR was also done which shows the presence of HPV DNA in the samples as HPV is considered as the causative factor behind cervical cancer. But the disadvantage of HPV PCR technique is that as HPV infection can be get cleared with time and a few percentage of normal samples may be predicted as positive for HPV DNA, also the sensitivity from HPV PCR is considered significantly low.

In conclusion, a label free ultrasensitive Raman fingerprint has been benchmarked to generate a well resolved biomolecular variation between the samples. Nucleic acids variations were confirmed by SERS analysis of extracted DNA while amino acid metabolites were validated by UFLC analysis. The results indicated the prevalence of nucleobases adenine, guanine, cytosine, phosphate backbone and amino acids tryptophan, phenyl alanine and proline which are the major metabolites evolved during tumorigenesis. Further spectral differentiation was validated by statistical analysis which included chemometric interpretations mainly by PCA, LDA and SVM. This is the first representation of SERS spectroscopic analysis in exfoliated cell samples. Moreover, the SERS based spectro-cytology was found to be minimally invasive and more sensitive than those employing serum or plasma as exfoliated cells represents a better source of sample for analyzing progression of cervical cancer. Taken together, the present strategy represents an accurate, simple and reliable method for the differential diagnosis of cervical cancer which might serve as a clinical detection technique in the near future. Also, we envision to store the reference data in a chip model (**Figure S8**) within a futuristic hand held Raman spectrometer for the screening of cervical cancer in large population.

Author contributions

V.K. and S.V.N. undertook all the synthesis and experimental studies. K.S.K and M.M.J helped in all chemometric analysis. G. S. and J.B.N helped in result interpretation and suggestions. K.G. R. contributed in intellectual content. All authors discussed the results and commented on the manuscript. K.K.M., K.S. and K. S.K. was responsible for the overall direction and coordination of the project.

Appendix A. Supplementary data

Supplementary data to this article can be found online at https://doi.org/10.1016/j.nano.2020.102276.

References

1. Cohen PA, Jhingran A, Oaknin A, Denny L. Cervical cancer. *Lancet* 2019;**393**:169-82, https://doi.org/10.1016/S0140-6736(18)32470-X.
2. Jess PRT, Smith DDW, Mazilu M, Dholakia K, Riches AC, Herrington CS. Early detection of cervical neoplasia by Raman spectroscopy. *Int J Cancer* 2007;**121**:2723-8, https://doi.org/10.1002/ijc.23046.
3. Fahey MT, Irwig L, Macaskill P. Meta-analysis of Pap test accuracy. *Am J Epidemiol* 1995;**141**:680-9, https://doi.org/10.1093/oxfordjournals.aje.a117485.
4. Solomon D, Davey D, Kurman R, Moriarty A, O'Connor D, Prey M, et al. The 2001 Bethesda system: terminology for reporting results of cervical cytology. *JAMA* 2002;**287**:2114-9, https://doi.org/10.1097/00006254-200208000-00015.
5. Boone JD, Erickson BK, Huh WK. New insights into cervical cancer screening. *J Gynecol Oncol* 2012;**23**:282-7, https://doi.org/10.3802/jgo.2012.23.4.282.
6. Sørbye SW, Suhrke P, Revå BW, Berland J, Maurseth RJ, Al-Shibli K. Accuracy of cervical cytology: comparison of diagnoses of 100 pap

smears read by four pathologists at three hospitals in Norway. *BMC Clin Pathol* 2017;**17**:1-6, https://doi.org/10.1186/s12907-017-0058-8.
7. Deepak RU, Kumar RR, Byju NB, Sharathkumar PN, Pournami C, et al. Computer assisted Pap smear analyser for cervical cancer screening using quantitative microscopy. *J Cytol Histol* 2015:S3, https://doi.org/10.4172/2157-7099.S3-010.
8. Cheng JX, Xie XS. Vibrational spectroscopic imaging of living systems: an emerging platform for biology and medicine. *Science* 2015;**350**(80): aaa88701 aa88709https://doi.org/10.1126/science.aaa8870.
9. Krishna CM, Sockalingum GD, Bhat Ra, Venteo L, Kushtagi P, Pluot M, et al. FTIR and Raman microspectroscopy of normal, benign, and malignant formalin-fixed ovarian tissues. *Anal Bioanal Chem* 2007;**387**:1649-56, https://doi.org/10.1007/s00216-006-0827-1.
10. Paidi SK, Diaz PM, Dadgar S, Jenkins SV, Quick CM, Griffin RJ, et al. Label-free Raman spectroscopy reveals signatures of radiation resistance in the tumor microenvironment. *Cancer Res* 2019;**79**:2054-64, https://doi.org/10.1158/0008-5472.CAN-18-2732.
11. Saranya G, Joseph MM, Karunakaran V, Nair JB, Saritha VN, Veena VS, et al. Enzyme-driven switchable fluorescence-SERS diagnostic nanococktail for the multiplex detection of lung Cancer biomarkers. *ACS Appl Mater Interfaces* 2018;**10**:38807-18, https://doi.org/10.1021/acsami.8b15583.
12. Movasaghi Z, Rehman S, Rehman IU. Raman spectroscopy of biological tissues. *Appl Spectrosc Rev* 2007;**42**:493-541, https://doi.org/10.1080/05704920701551530.
13. Kumar S, Rizwan A, Zheng C, Cheng M, Glunde K, Barman I. Label-free Raman spectroscopy detects stromal adaptations in Premetastatic lungs primed by breast Cancer. *Cancer Res* 2017;**77**:247-56.
14. Krishna CM, Prathima NB, Malini R, Vadhiraja BM, Bhatt RA, Fernandes DJ, et al. Raman spectroscopy studies for diagnosis of cancers in human uterine cervix. *Vib Spectrosc* 2006, https://doi.org/10.1016/j.vibspec.2006.01.011.
15. Chen PH, Shimada R, Yabumoto S, Okajima H, Ando M, Chang CT, et al. Automatic and objective oral cancer diagnosis by Raman spectroscopic detection of keratin with multivariate curve resolution analysis. *Sci Rep* 2016;**6**:1-9, https://doi.org/10.1038/srep20097.
16. Duraipandian S, Bergholt MS, Zheng W, Ho KY, Teh M, Yeoh KG, et al. Real-time Raman spectroscopy for in vivo, online gastric cancer diagnosis during clinical endoscopic examination. *J Biomed Opt* 2012;**17**081418, https://doi.org/10.1117/1.JBO.17.
17. Meksiarun P, Ishigaki M, Huck-Pezzei VAC, Huck CW, Wongravee K, Sato H, et al. Comparison of multivariate analysis methods for extracting the paraffin component from the paraffin-embedded cancer tissue spectra for Raman imaging. *Sci Rep* 2017;**7**:1-10, https://doi.org/10.1038/srep44890.
18. Huefner A, Kuan WL, Müller KH, Skepper JN, Barker RA, Mahajan S. Characterization and visualization of vesicles in the endo-lysosomal pathway with surface-enhanced Raman spectroscopy and chemometrics. *ACS Nano* 2016;**10**:307-16, https://doi.org/10.1021/acsnano.5b04456.
19. Shin H, Jeong H, Park J, Hong S, Choi Y. Correlation between cancerous exosomes and protein markers based on surface-enhanced Raman spectroscopy (SERS) and principal component analysis (PCA). *ACS Sensors* 2018;**3**:2637-43, https://doi.org/10.1021/acssensors.8b01047.
20. Hutchings J, Kendall C, Shepherd N, Barr H, Stone N. Evaluation of linear discriminant analysis for automated Raman histological mapping of esophageal high-grade dysplasia. *J Biomed Opt* 2010;**15**066015, https://doi.org/10.1117/1.3512244.
21. Sattlecker M, Bessant C, Smith J, Stone N. Investigation of support vector machines and Raman spectroscopy for lymph node diagnostics. *Analyst* 2010;**135**:895-901, https://doi.org/10.1039/b920229c.
22. Langer J, Jimenez de Aberasturi D, Aizpurua J, Alvarez-Puebla RA, Auguié B, Baumberg JJ, et al. Present and future of surface-enhanced Raman scattering. *ACS Nano* 2019, https://doi.org/10.1021/acsnano.9b04224.
23. Jimenez De Aberasturi D, Serrano-Montes AB, Langer J, Henriksen-Lacey M, Parak WJ, Liz-Marzán LM. Surface enhanced Raman scattering encoded gold Nanostars for multiplexed cell discrimination. *Chem Mater* 2016;**28**:6779-90, https://doi.org/10.1021/acs.chemmater.6b03349.
24. Kneipp J, Kneipp H, McLaughlin M, Brown D, Kneipp K. In vivo molecular probing of cellular compartments with gold nanoparticles and Nanoaggregates. *Nano Lett* 2006;**6**:2225-31, https://doi.org/10.1021/nl061517x.
25. Panikkanvalappil SR, Hira SM, Mahmoud MA, El-Sayed MA. Unraveling the biomolecular snapshots of mitosis in healthy and cancer cells using plasmonically-enhanced Raman spectroscopy. *J Am Chem Soc* 2014;**136**:15961-8, https://doi.org/10.1021/ja506289u.
26. Kang B, Austin L a, El-Sayed M a. Observing molecular events in real-time of apoptosis dynamics in living cancer cells using nuclear targeted plasmonically enhanced Raman nanoprobes. *ACS Nano* 2014:4883-92, https://doi.org/10.1021/nn500840x.
27. Gonz^|^aacute;lez-Sol^|^iacute;s J, Lu^|^eacute;vano-Colmenero G, Vargas-Mancilla J. Surface enhanced Raman spectroscopy in breast cancer cells. LASER Ther 2013. https://doi.org/10.5978/islsm.13-OR-05.
28. Li S, Li L, Zeng Q, Zhang Y, Guo Z, Liu Z, et al. Characterization and noninvasive diagnosis of bladder cancer with serum surface enhanced Raman spectroscopy and genetic algorithms. *Sci Rep* 2015;**5**:9582, https://doi.org/10.1038/srep09582.
29. Chen Y, Zhang Y, Pan F, Liu J, Wang K, Zhang C, et al. Breath analysis based on surface-enhanced Raman scattering sensors distinguishes early and advanced gastric Cancer patients from healthy persons. *ACS Nano* 2016;**10**:8169-79, https://doi.org/10.1021/acsnano.6b01441.
30. Feng S, Wang W, Tai IT, Chen G, Chen R, Zeng H. Label-free surface-enhanced Raman spectroscopy for detection of colorectal cancer and precursor lesions using blood plasma. *Biomed Opt Express* 2015;**6**:3494, https://doi.org/10.1364/BOE.6.003494.
31. Yan B, Li B, Wen Z, Luo X, Xue L, Li L. Label-free blood serum detection by using surface-enhanced Raman spectroscopy and support vector machine for the preoperative diagnosis of parotid gland tumors. *BMC Cancer* 2015;**15**:650, https://doi.org/10.1186/s12885-015-1653-7.
32. Mert S, Özbek E, Ötünçtemur A, Çulha M. Kidney tumor staging using surface-enhanced Raman scattering. *J Biomed Opt* 2015;**20**047002, https://doi.org/10.1117/1.JBO.20.4.047002.
33. González-Solís JL, Martínez-Espinosa JC, Torres-González LA, Aguilar-Lemarroy A, Jave-Suárez LF, Palomares-Anda P. Cervical cancer detection based on serum sample Raman spectroscopy. *Lasers Med Sci* 2014;**29**:979-85, https://doi.org/10.1007/s10103-013-1447-6.
34. Rubina S, Amita M, Kedar KD, Bharat R, Krishna CM. Raman spectroscopic study on classification of cervical cell specimens. *Vib Spectrosc* 2013, https://doi.org/10.1016/j.vibspec.2013.06.002.
35. Lyng FM, O'Leary JJ, Traynor D, Martin CM, Kearney P, Bonnier F. Raman spectral signatures of cervical exfoliated cells from liquid-based cytology samples. *J Biomed Opt* 2017;**22**:1, https://doi.org/10.1117/1.jbo.22.10.105008.
36. Traynor D, Kearney P, O'Leary JJ, Lyng FM, Martin C, Duraipandian S. Raman spectroscopic detection of high-grade cervical cytology: using morphologically normal appearing cells. *Sci Rep* 2018;**8**:1-8, https://doi.org/10.1038/s41598-018-33417-8.
37. Duraipandian S, Mo J, Zheng W, Huang Z. Near-infrared Raman spectroscopy for assessing biochemical changes of cervical tissue associated with precarcinogenic transformation. *Analyst* 2014;**139**:5379-86, https://doi.org/10.1039/c4an00795f.
38. Low JJH, Ilancheran A, Ng J, Zheng W, Huang Z, Duraipandian S. Simultaneous fingerprint and high-wavenumber confocal Raman spectroscopy enhances early detection of cervical Precancer in vivo. *Anal Chem* 2012;**84**:5913-9, https://doi.org/10.1021/ac300394f.
39. Feng S, Lin D, Lin J, Li B, Huang Z, Chen G, et al. Blood plasma surface-enhanced Raman spectroscopy for non-invasive optical detection of cervical cancer. *Analyst* 2013;**138**:3967-74, https://doi.org/10.1039/c3an36890d.
40. S.A. Sanchez-Rojo ´ a, B.E. Mart'ınez-Zeregaa, E.F. Velazquez-Pedroza ´ a, J.C. Mart'ınez-Espinosab LAT-G´ c, A. Aguilar-Lemarroyd, L.F.

Jave-Suarez ´ d PP-A and JLG-S´ ´ıs. Cervical cancer detection based on serum sample surface enhanced Raman spectroscopy. Rev Mex F'ısica 2016;62:213–218. https://doi.org/10.1007/s10103-013-1447-6.

41. Kim ES, Samanta A, Cheng HS, Ding Z, Han W, Toschi L, et al. Effect of oncogene activating mutations and kinase inhibitors on amino acid metabolism of human isogenic breast cancer cells. *Mol Biosyst* 2015;**11**:3378-86, https://doi.org/10.1039/c5mb00525f.
42. Njoki PN, Lim IIS, Mott D, Park HY, Khan B, Mishra S, et al. Size correlation of optical and spectroscopic properties for gold nanoparticles. *J Phys Chem C* 2007;**111**:14664-9, https://doi.org/10.1021/jp074902z.
43. Stamplecoskie KG, Scaiano JC, Tiwari VS, Anis H. Optimal size of silver nanoparticles for surface-enhanced Raman spectroscopy. *J Phys Chem C* 2011;**115**:1403-9, https://doi.org/10.1021/jp106666t.
44. Polte J, Ahner TT, Delissen F, Sokolov S. Mechanism of gold nanoparticle formation in the classical citrate synthesis method derived from coupled in situ XANES and SAXS evaluation. *J Am Chem Soc* 2010;**132**:1296-301, https://doi.org/10.1021/ja906506j.
45. David C. *Wilbur MB*. III: Comprehensive Cytopathology; 2008.
46. Kuku G, Altunbek M, Culha M. Surface-enhanced Raman scattering for label-free living single cell analysis. *Anal Chem* 2017;**89**:11160-6, https://doi.org/10.1021/acs.analchem.7b03211.
47. Sujai PT, Joseph MM, Saranya G, Nair JB, Murali VP, Maiti KK. Surface charge modulates the internalization: Vs. penetration of gold nanoparticles: comprehensive scrutiny on monolayer cancer cells, multicellular spheroids and solid tumors by SERS modality. *Nanoscale* 2020;**12**:6971-5, https://doi.org/10.1039/d0nr00809e.
48. Yooa KM, Zhub HR, Akinsb DL, Prudented R, Celmerd E, Carond A, et al. Raman, fluorescence, and time-resolved light scattering as optical diagnostic techniques to separate diseased and normal biomedical media. *J Photochem Photobiol B Biol* 1992;**16**:187-209.
49. Shen T, Guo Q. Role of Pyk2 in human cancers. *Med Sci Monit* 2018;**24**:8172-82, https://doi.org/10.12659/MSM.913479.
50. Kuang BH, Zhang MQ, Xu LH, Hu LJ, Wang HB, Zhao WF, et al. Proline-rich tyrosine kinase 2 and its phosphorylated form pY881 are novel prognostic markers for non-small-cell lung cancer progression and patients' overall survival. *Br J Cancer* 2013;**109**:1252-63, https://doi.org/10.1038/bjc.2013.439.
51. Fendt S, Verfaillie C, Gru TGP. Proline metabolism supports metastasis formation and could be inhibited to selectively target metastasizing cancer cells. *Nat Commun* 2017;**8**, https://doi.org/10.1038/ncomms15267.
52. Liu W, Hancock CN, Fischer JW, Harman M, Phang JM. Proline biosynthesis augments tumor cell growth and aerobic glycolysis : involvement of pyridine nucleotides. *Sci Rep* 2015;**5**, https://doi.org/10.1038/srep17206.
53. Kübler K, Heinenberg S, Rudlowski C, Keyver-Paik MD, Abramian A, Merkelbach-Bruse S, et al. C-Myc copy number gain is a powerful prognosticator of disease outcome in cervical dysplasia. *Oncotarget* 2015;**6**:825-35, https://doi.org/10.18632/oncotarget.2706.
54. Gottschalk EY, Meneses PI. A dual role for the nonreceptor tyrosine kinase Pyk2 during the intracellular trafficking of human Papillomavirus 16. *JVirol* 2015;**89**:9103-14, https://doi.org/10.1128/JVI.01183-15.
55. Chen Y, Dai J, Zhou X, Liu Y, Zhang W, Peng G. Raman spectroscopy analysis of the biochemical characteristics of molecules associated with the malignant transformation of gastric mucosa. *PLoS One* 2014;**9**e93906, https://doi.org/10.1371/journal.pone.0093906.
56. Ayre WB, Ayre JE. Cytochemical study of glycogen in the diagnosis of cervical cancer. *Am J Clin Pathol* 1950;**20**:644-50, https://doi.org/10.1093/ajcp/20.7.644.
57. Gregoire AT, Ledger WD, Moran MJ. The glycogen content of the human female genital tract in cycling, menopausal, and women with Encometrial and cervical carcinoma. Fertil Steril 2016;24:198–201. https://doi.org/10.1016/s0015-0282(16)39553-x.
58. Su PF, Wu FYH. Differential suppression of the tumorigenicity of HeLa and SiHa cells by adeno-associated virus. *Br J Cancer* 1996;**73**:1533-7, https://doi.org/10.1038/bjc.1996.289.